CHEMISTRY OF MATERIALS

pubs.acs.org/cm

Review

Recent Advances in Heterosilica-Based Micro/Nanomotors: Designs, Biomedical Applications, and Future Perspectives

Miao Yan, Lei Xie, Jinyao Tang, Kang Liang, Yongfeng Mei, and Biao Kong*

Cite This: *Chem. Mater.* 2021, 33, 3022−3046

Read Online

ACCESS | Metrics & More | Article Recommendations

ABSTRACT: The development of self-propelled micro/nanomotors (MNMs) has presented a variety of opportunities in the biomedical field because of their surprisingly high performance. However, the biosafety and feasibility of MNMs is still far from satisfactory for disease treatment in clinical application. Silica is one of the most extensively used material for the construction of versatile MNMs and has been intensively applied in the biomedical field due to their excellent biocompatibility, negligible cytotoxicity, and tailorable physiochemical properties such as stimuli-responsive behavior, controllable particle size, surface topology, shape, and mesostructure as well as conjugating targeting molecules and/or gatekeepers to endow enhanced cellular internalization, improved cell selectivity, and on-demand release. Heterosilica-based MNMs, a class of silica-based structures incorporated with diverse functional units and materials, exhibit new burgeoning possibilities for practical biomedical applications. These functional units and compositions substantially created an enormous impact on improving the motion performances and morphological features of MNMs. In this review, we present a systematic overview of the development of the heterosilica-based MNM systems. The discussion is mainly focused on the design and construction of diverse heterosilica-based engines. Meanwhile, we also highlight the effects of key parameters on their performance such as surface properties. Then, we summarize their biomedical applications. We further provide an outlook toward future developments of the heterosilica-based MNMs. This review is expected to inspire further development in future biomedical applications.

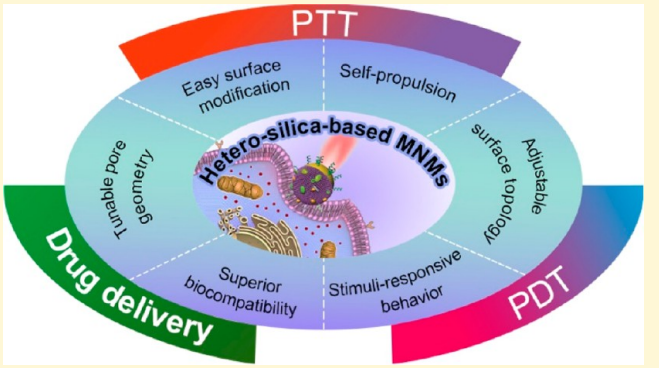

INTRODUCTION

In the realm of biology, biomolecular motors, such as motor protein kinesin or myosin, are natural machines with the ability to fulfill intricate tasks by converting biochemical fuel into mechanical movement.[1−3] Inspired by these intriguing phenomena, scientists from multiple disciplines attempt to synthesize artificial molecular machines to realize controlled manipulation at the molecular level, and many sophisticated nanomachines with advanced structures, such as molecular shuttles, molecular cables, molecular rotors, and molecular elevators, have been engineered.[4] Because of their profound application potential in manipulating and manufacturing entities at the molecular scale, the molecular motors have been awarded a Nobel Prize for Chemistry in 2016.[5,6] To achieve motion on the nanometer/micrometer scale, extensive effort has been devoted to fabrication, design, and performance improvement of MNMs. They can be powered in diverse fluids by converting other forms of energy such as chemical fuel, light, magnetic or electric fields, and ultrasonic waves into mechanical energy to achieve autonomous movement. These artificial MNMs are normally designed to be asymmetric in geometry or surface chemistry to achieve a translation movement such as Janus motors, sphere motors, bowl motors, tube motors, bottle motors, spiral motors, or wire motors,[7−15] etc. MNMs show great capability of precise control over both direction and velocity of movement. As a result, they can perform complicated tasks that passive devices cannot fulfill. For instance, by integrating self-propulsion and navigation capabilities, MNMs not only achieve targeted delivery of drugs to predefined sites of the body but also facilitate cell/tissue penetration.[16,17] Therefore, the advent of MNMs offers enormous possibilities for use in in vitro and in vivo applications.[18,19]

Although considerable efforts have led to the tremendous progress in the biomedical field, there are still many challenges remaining in the fabrication, performance, and clinical use of

Received: January 21, 2021
Revised: March 13, 2021
Published: April 22, 2021

Scheme 1. Schematic Illustrating the Synthetic Strategies, Architectures, and Biomedical Applications of Heterosilica-Based MNMs[a]

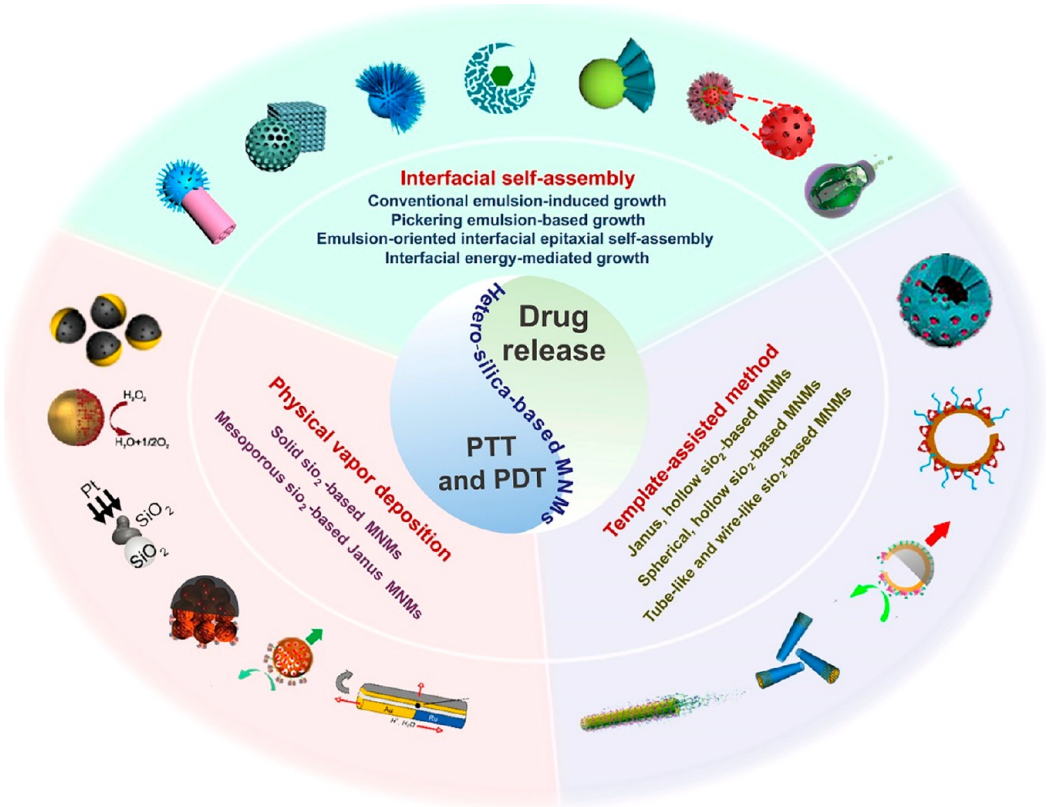

[a]Reprinted with permission from ref 25. Copyright 2014 American Chemical Society. Reprinted with permission from ref 56. 2009 American Chemical Society. Reprinted with permission from ref 60. 2015 The Royal Society of Chemistry. Reprinted with permission from ref 70. 2018 Wiley-VCH Verlag. Reprinted with permission from ref 73. 2015 The Royal Society of Chemistry. Reprinted with permission from ref 75. 2017 Elsevier Ltd. Reprinted with permission from ref 81. 2019 Elsevier Inc. Reprinted with permission from ref 82. 2015 American Chemical Society. Reprinted with permission from ref 86. 2015 American Chemical Society. Reprinted with permission from ref 87. 2016 American Chemical Society. Reprinted with permission from ref 91. 2019 American Chemical Society. Reprinted with permission from ref 94. 2016 American Chemical Society. Reprinted with permission from ref 95. 2017 Springer Nature. Reprinted with permission from ref 96. 2016 Wiley-VCH Verlag. Reprinted with permission from ref 102. 2017 American Chemical Society. Reprinted with permission from ref 103. 2020 Wiley-VCH Verlag. Reprinted with permission from ref 107. 2020 Elsevier Inc. Reprinted with permission from ref 121. 2020 American Chemical Society.

MNMs. The structures and components of the existing MNMs lack diversity, which limits them to perform specific functions.[20] Designing and constructing MNMs with required functionality, excellent biocompatibility, desirable structures, high degrees of complexity and anisotropy, and more potential structures is still urgently desired. Hence, a robust and versatile matrix is crucial for designing sophisticated MNMs systems.

Silica is considered an ideal platform for synthetic MNMs components for biomedical usage. Nowadays, silica is the most widely used material in biomedical field due to its good biocompatibility and negligible cytotoxicity.[21] It is nontoxic and "generally recognized as safe" (GRAS) by the U.S. Food and Drug Administration for use in food additives and vitamin supplements.[22] Compared with other materials, the inert nature of the silica matrix against chemicals creates a fascinating platform to construct MNMs for biomedical usage.[23] Silica also possesses other attractive features such as ease in producing large-scale monodisperse colloids with controllable diameters, mechanical and chemical stabilities, stimuli-responsive behavior, modified surface properties, and ability to be integrated with metals or biocomponents.[21,24] In addition, silica materials, with controllable mesoporous structures, have been widely synthesized using the surfactants-mediated self-assembly method.[24,25] Due to their tunable pore size, large pore volume, high drug loading capacity, mesoporous silica structures have already been considered as a scaffold for the preparation of versatile heterosilica-based MNMs; they can effectively load and transport biomedical reagents toward targeted locations for precise drug release.[26,27] Depending on the types of loaded drugs, various therapeutical purposes can be achieved, which endows them with more flexibility in cancer treatment. So far, diverse heterosilica-based MNMs have been developed based on different propulsion mechanisms, including bubble propulsion,[28,29] surface tension gradients,[30] self-thermophoresis,[31,32] self-electrophoresis,[33] and self-diffusiophoresis.[34] Due to the ease of surface modification of silica materials, diverse biomimetic heterosilica-based MNMs by employing cellular components (e.g., motile tissues and microorganisms) are successfully designed and present a dramatic increase of the MNMs biocompatibility and biodegradability. Such fully biocompatible biohybrid MNMs not only prolong the circulation time of MNMs in biofluids but also effectively prevent undesired immune attacks from the human body.[35] Moreover, the easy surface coating of mesoporous silica endows them with the ability to anchor stimuli-responsive gated molecules (e.g., supramolecular

https://doi.org/10.1021/acs.chemmater.1c00192
Chem. Mater. 2021, 33, 3022−3046

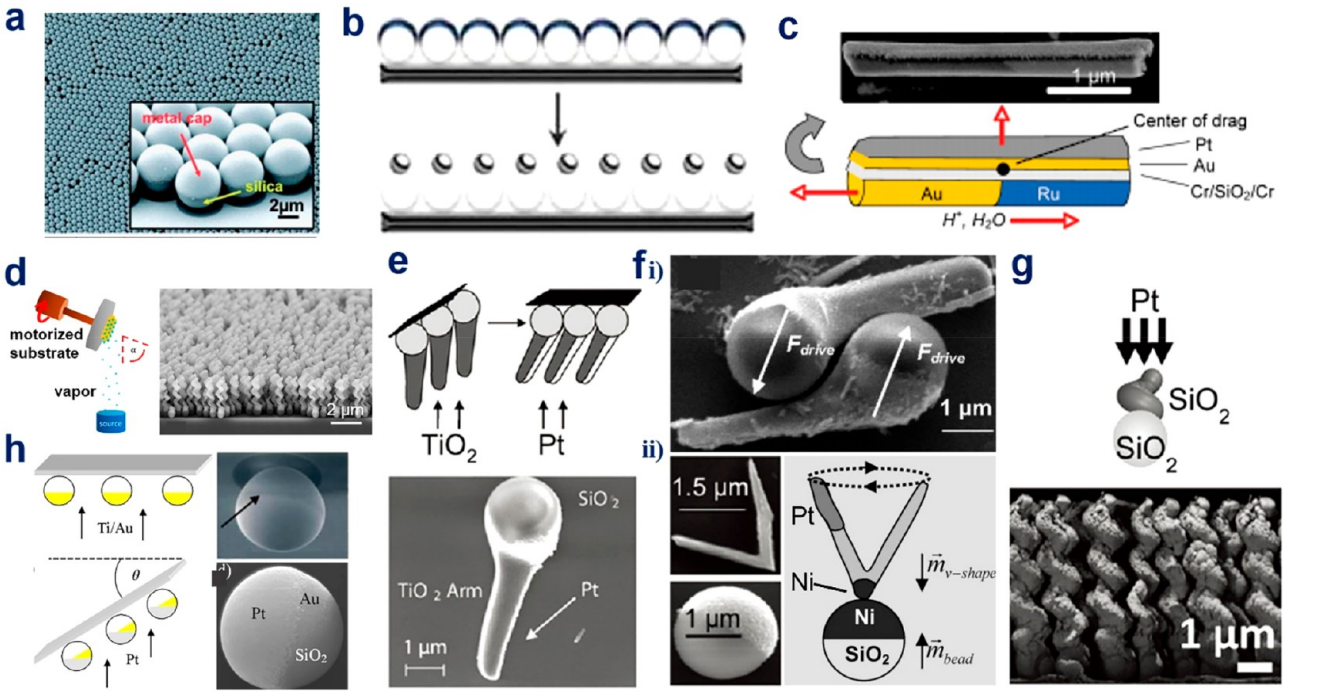

Figure 1. Schematic of preparation process of heterosilica-based MNMs with various structures by the PVD and GLAD techniques. (a) SEM images of metal-SiO_2 Janus-type MNMs. Reprinted with permission from ref 54. Copyright 2012 American Chemical Society. (b) Schematic illustration of the synthesis process of a catalytic dimer motor composed of a silica sphere and a platinum sphere. Reprinted with permission from ref 55. Copyright 2010 Wiley-VCH Verlag. (c) Illustration of rodlike multicomponent motor. Reprinted with permission from ref 56. Copyright 2009 American Chemical Society. (d) Helices grow on the SiO_2 seeds by azimuthal rotation of a tilted substrate stage during deposition. Reprinted with permission from ref 57. Copyright 2013 American Chemical Society. (e) TiO_2 and Pt are deposited onto the SiO_2 microbeads at an angle. Reprinted with permission from ref 58. Copyright 2009 Wiley-VCH Verlag. (f) (i) Interlocked tadpole shaped nanomotors and (iii) helicopter motors by assembly of V-shaped Pt/TiO_2/Ni nanorods and Ni-coated SiO_2 Janus sphere. Reprinted with permission from ref 59. Copyright 2010 Wiley-VCH Verlag. (g) Schematic illustration of the deposition process of catalytic microdrills. Reprinted with permission from ref 60. Copyright 2015 The Royal Society of Chemistry. (h) Synthesis of asymmetric bimetallic Pt/Au-coated catalytic micromotors. Reprinted with permission from ref 61. Copyright 2010 American Institute of Physics.

systems) and/or active targeting ligands to further improve the therapeutic efficiency of drugs and reduce the side effects toward normal cells. Therefore, these fascinating and promising heterosilica-based MNMs are expected to perform diverse biomedical tasks such as directed drug delivery, biopsy, local diagnosis, precision nanosurgery, and bioimaging.[36]

Although numerous reports based on MNMs have been reviewed, they have mainly focused on propulsion mechanisms or applications.[37−42] Few literature reports have put emphasis on the synthesis methodologies and biocompatibility of MNMs, and a review topic on heterosilica-based MNMs is particularly rare. Herein, we carefully review the latest progress of heterosilica-based MNMs, and the discussion is focused on the construction methodologies based on silica materials with diverse structures and their application in the biomedical field. The review is organized into four sections (Scheme 1): First, a brief development history of MNMs is introduced. Then, we give a comprehensive overview of construction methodologies of heterosilica-based MNMs including (i) physical vapor deposition technique (PVD), (ii) template-assisted method, and (iii) interfacial assembly strategy. The core principle of these approaches is to build asymmetry of geometry, composition, or surface properties. Notably, with regard to the interfacial assembly strategy, interfacial-energy-mediated assembly is also introduced for the construction of future heterosilica-based MNMs with more advanced and sophisticated structures, which are not specifically designed for MNMs applications. However, they endow MNMs with more flexibility in design, fabrication, and control of motion performance and demonstrate considerable promise for biomedical applications. The third section presents an overview of the biomedical applications of the heterosilica-based MNMs including targeted drug delivery based on various propulsion mechanisms, photothermal cancer therapy (PTT), and photodynamic therapy (PDT). Finally, a summary and outlook on the major challenges and future opportunities of these heterosilica-based MNMs in practical biochemical applications are proposed.

2. DESIGN AND SYNTHETIC STRATEGIES OF HETEROSILICA-BASED MNMS

In the following section, we will provide a brief overview of the existing design and fabrication methods of heterosilica-based MNMs before we discuss their applications in biomedical applications. Nowadays, achieving precise control over velocity and direction of MNMs remains an intriguing challenge. MNMs experience drag force when functioning in a micro/nanometer regime and a viscous biological media.[43] In this case, Brownian motion becomes more dominant, and the inertia forces are no longer possible for driving the movement of the MNMs.[44] Therefore, careful design is of importance for future realistic applications in the biomedical field.

First, constructing asymmetries in geometry or surface chemistry is expected to change the experienced drag force in

https://doi.org/10.1021/acs.chemmater.1c00192
Chem. Mater. 2021, 33, 3022−3046

biological media, which can asymmetrically accumulate products to form a net driving force for directed motion of MNMs. On the other hand, some other factors also should be considered including cost, scalability, biocompatibility, etc. Here we intend to illustrate various construction methodologies with representative examples. Additionally, we also discuss their advantages/disadvantages of different fabrication strategies. In general, synthetic strategies of heterosilica-based MNMs can be broadly classified as PVD technique, template-assisted approach, and interfacial assembly method.

2.1. Physical Vapor Deposition. PVD is the most convenient and controllable technique to deposit a thin and homogeneous coating on the substrate, which is in the form of vapor particles from a material source (target).[45] In this process, the source material (target) is vaporized and released into gas by bombardment of an electron beam (e-beam) or ionized argon gas. Then the atoms are deposited on the surface of the substrates in a vacuum or partial vacuum and thus forming a thin film. It is possible to obtain multilayer functions on the substrate by adjusting the source material. Common types of PVD processes include e-beam evaporation deposition and sputtering deposition. The PVD method is typically used to deposit metals.[46] However, oxides or semiconductors can also be deposited utilizing e-beam evaporation.

It is also possible to prepare multicomponent materials by the PVD technique, which can incorporate one or several target materials into micro/nanostructures. This method is extensively used in the fabrication processes of multifunctional MNMs. A suitable micro/nanostructure is first chosen to provide a template for deposition of target materials. By the virtues of unique structure, colloidal stability, allowing large-scale production, excellent biocompatibility, and easy surface functionalization, silica has been regarded as an ideal platform to deposit target materials. By introducing target materials with magnetic or catalytic properties or inert materials for achieving asymmetric reaction, various heterosilica-based MNMs are designed. In this section, we will demonstrate synthetic heterosilica-based MNMs by conventional PVD and its variation, glancing angle deposition (GLAD).

2.1.1. Solid Silica Sphere and Physical Vapor Deposition Method. Janus-type structures have been employed to prepare MNMs due to their distinguished surface properties, which can produce a "'net force'" to propel the movement of motors, such as catalytic reaction induced bubble propulsion, neutral self-diffusiophoresis, or electrolyte/ionic self-diffusiophoresis.[47−53] For catalytic Janus-type MNMs, the most common one is to deposit metallic species with active catalytic components on a monolayer of spherical silica particles to form islands or hemispherical caplike structures by PVD. During this process, partial shielding is required to ensure the asymmetry of the structures. The obtained Janus-type spherical motors can accumulate anisotropically products, which results in directional motion of the motors (Figure 1a).[54] Besides the spherical motors, PVD can be used to fabricate other motors with diverse morphologies. Valadares et al. reported a catalytic dimer motor, which was composed of a silica sphere and a platinum sphere. The spheres were first coated with a bilayer of chromium (Cr)/platinum (Pt) by sputtering, followed by the metallic bilayer half-shell dewetting by an annealing process, and thus forming a platinum particle connected to each silica sphere (Figure 1b).[55] Another typical example is a rodlike motor fabricated by PVD. First, Cr, SiO_2, Cr, Au, and Pt layers were sequentially deposited on one side of the Au−Ru bimetallic rod by PVD. After that, the second Au/Pt catalytic bilayer adds a perpendicular force that results in ∼10 times faster rotation than previously reported. (Figure 1c).[56]

Besides the vapor flux components change, the vapor flux or substrate angle can set at the tilting angle (glancing angle). Various complex three-dimensional MNMs can be obtained by manipulating the tilt and rotation of the substrate relative to the incoming vapor flux during deposition. Figure 1d demonstrates the helical structure by the GLAD technique. To obtain uniform helical structures, an array of ordered silica spheres was used as seeds and placed on the surface of the substrate. After that, helices grew on the seeds by azimuthal rotation of a tilted substrate stage during deposition.[57] Using the dynamic shadow growth strategy, Gibbs et al. grew Pt/TiO_2 rods on silica spheres (Figure 1e).[58] Furthermore, interlocked tadpole-shaped nanomotors (Figure 1f (i)) or helicopter motors ((Figure 1f (ii)) assembled by V-shaped Pt/TiO_2/Ni nanorods and Ni-coated SiO_2 Janus sphere by either van der Waals or magnetic interactions were also fabricated, and these assembled structures demonstrated different rotation abilities.[59] In the following study, Gibbs and Fischer designed catalytic microdrills through GLAD.[60] As shown in Figure 1g, a turn of the SiO_2 helix with a diameter of 400 ± 200 nm was deposited on a SiO_2 sphere to form a helical structure and was further asymmetrically coated with Pt. This process was repeated several times until the helical catalytic microdrills were fabricated. To obtain an asymmetric bimetallic coating, an Au/Ti metallic bilayer was deposited followed by the substrate with silica spheres rotated to a polar angle, and the Pt was deposited on the exposed Au layer.[61] This special structure can adjust motion behaviors by varying the exposed area of the Au layer (Figure 1h).

2.1.2. Mesoporous Silica Nanoparticles (MSNs) and Physical Vapor Deposition Method. Compared to conventional solid Janus micromotors, MSNs, due to their unique structure, tunable pore size, large pore volume, high drug loading capacity, excellent biocompatibility, and easy surface modification have been widely investigated in the biomedical field during the past decades.[62] As is well-known, mesoporous silica nanomaterials have been employed as nanocarriers to load different cargoes for various purposes.[62−64] For instance, some anticancer drug molecules were loaded inside the pores of silica, then delivered into cancer cells by endocytosis.[65] Photosensitizers or fluorescent dyes can also be chemisorbed or physically absorbed on the surface or channel for bioimaging or photodynamic therapy in cancer treatment.[63,66] These processes were achieved mainly in passive delivery behaviors. In order to achieve active target delivery, MNMs have emerged as new-generation smart drug-delivery vehicles that are capable of loading and transporting therapeutic reagents by self-propelled movement, which improves drug delivery efficiency and shortens the transportation time in the blood circulation.[35] When integrating with remote steering by a magnetic field, movement direction can be controlled more precisely, thus enabling motors to actively seek and enter the site of interest.[20,67,68] Such a strategy can directly transport drugs to cancer cells in an active manner and therefore brings a promising future to nanomedicine field.

At present, Janus-type heterosilica-based MNMs are one of the most widely used in biomedicine fields, which are composed of a mesoporous silica sphere and metal half-shells by PVD.[43,69] The ordered mesoporous silica materials are synthesized by the sol−gel procedures, which involve the

https://doi.org/10.1021/acs.chemmater.1c00192
Chem. Mater. 2021, 33, 3022−3046

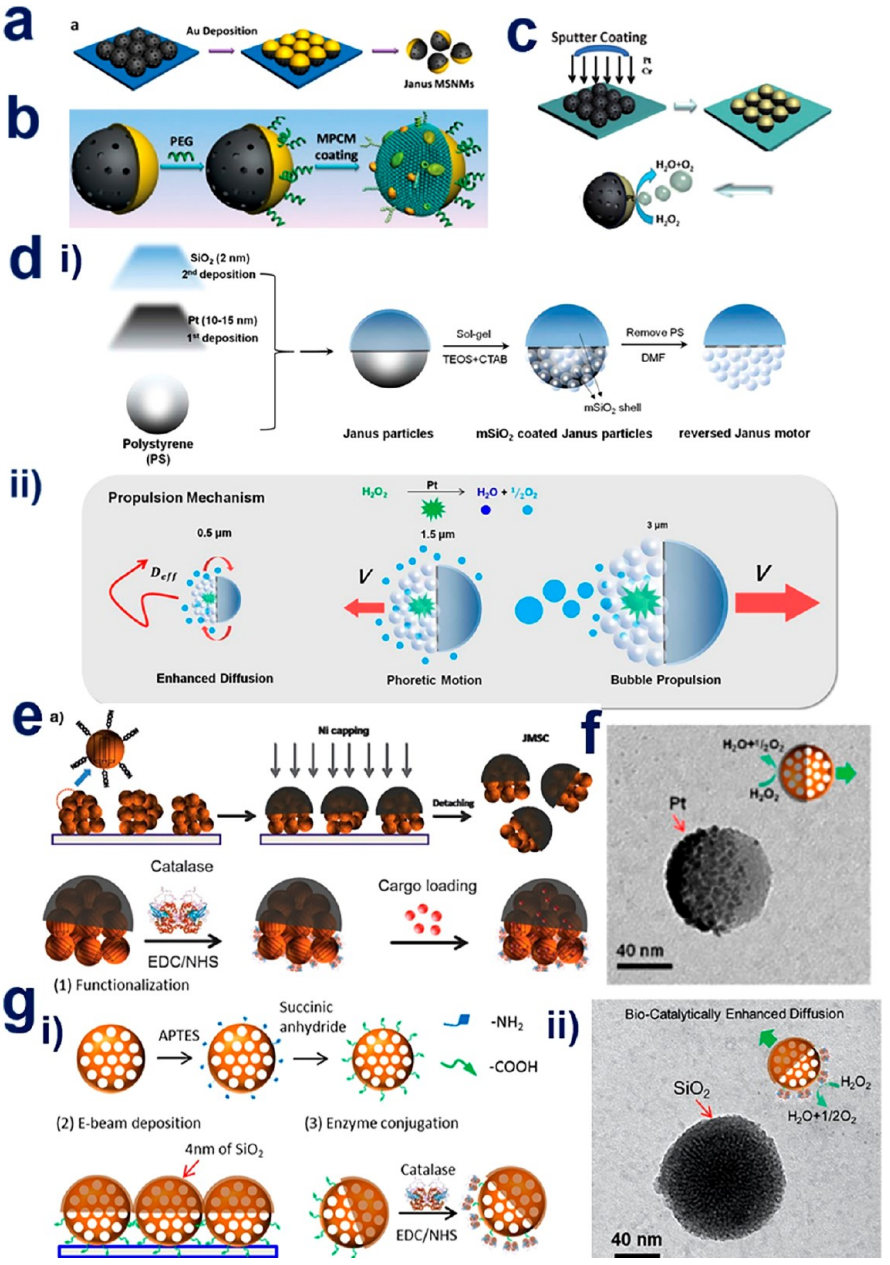

Figure 2. Synthetic mesoporous Janus heterosilica-based MNMs by PVD techniques. (a) Schematic illustration of fabrication and SEM images (scale bar = 200 nm) of the Au-SiO_2 Janus nanomotors. The insets show corresponding TEM images (scale bar = 20 nm). Reprinted with permission from ref 32. Copyright 2016 American Chemical Society. (b) Schematic illustration of the preparation of the MPCM-camouflaged Au-SiO_2 Janus nanomotor. Reprinted with permission from ref 70. Copyright 2018 Wiley-VCH Verlag. (c) Preparation of biotin-modified Pt-SiO_2 Janus micromotors. Reprinted with permission from ref 71. Copyright 2014 Wiley-VCH Verlag. (d) (i) Material development of the reversed Janus nanomotor and (ii) size-dependent movement behavior. Reprinted with permission from ref 72. Copyright 2016 American Chemical Society. (e) Schematic illustration of Ni-coated SiO_2 cluster Janus motors' fabrication and cargo loading. Reprinted with permission from ref 73. (f) TEM image of Pt-SiO_2 Janus and inset display catalyst Pt-triggered the decomposition of H_2O_2 for self-propulsion of nanomotors. Reprinted with permission from ref 43. Copyright 2015 American Chemical Society. (g) (i) Fabrication scheme of biocatalytic Janus mesoporous silica nanomotors and (ii) schematically illustrating enhanced diffusion of a biocatalytic Janus motor. Reprinted with permission from ref 75. Copyright 2017 Elsevier Ltd.

successive hydrolysis and condensation of silica precursor.[24] In this process, assembled cationic surfactant micelle templates were used as structure-directing agents for polymerizing the silica component by electrostatic interaction.[25] Xuan et al. recently presented a mesoporous silica/Au Janus nanomotor with tunable sizes ranging from 50 to 120 nm.[32] As illustrated in Figure 2a, the as-synthesized SiO_2 spheres show ordered pore channels. The MSNs were first spread on a substrate, for example, silicon slide, to form a two-dimensional MSN monolayer and was subsequently coated with a 10 nm Au layer by the PVD technique. The obtained Au half-shells Janus nanoparticles demonstrated fuel-free, NIR-driven swimming behavior due to the photothermal effect of the AuNSs. NIR-powered nanomotors provide potential cargo transportation in a biofriendly manner. In biological medium, it is difficult to achieve locomotion for synthetic nanomotors without interfacing features because of the ubiquitous bioadhesion in living organisms and thus failing to perform active targeted

https://doi.org/10.1021/acs.chemmater.1c00192
Chem. Mater. 2021, 33, 3022−3046

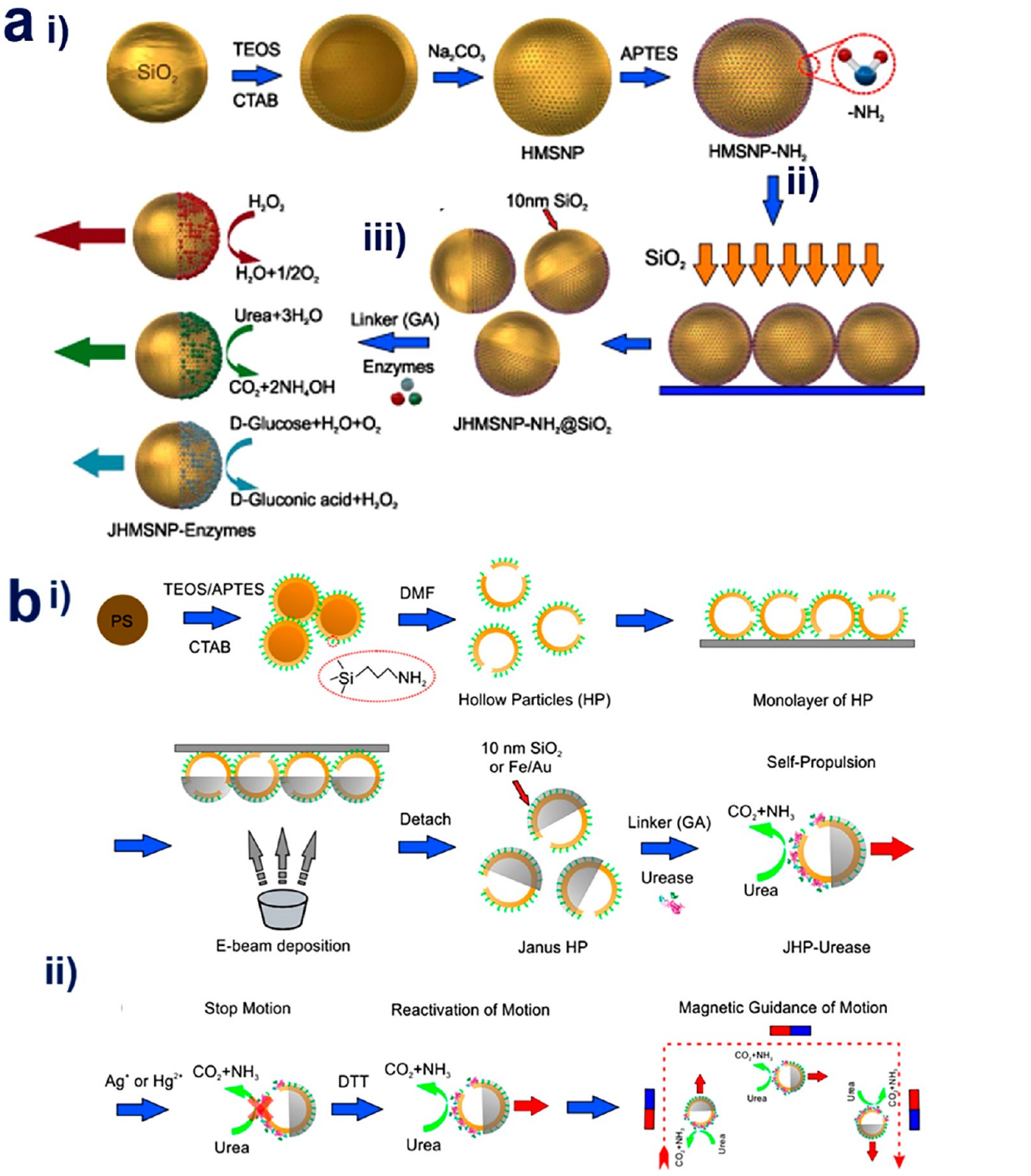

Figure 3. Janus, hollow heterosilica-based MNMs. (a) Schematic illustration of the fabrication of hollow Janus-type MSNs and conjugation of enzymes (gatalase, glucose oxidase (GOx), and urease) onto one side of the Janus nanoparticles via a glutaraldehyde (GA) linker. Reprinted with permission from ref 86. Copyright 2015 American Chemical Society. (b) (i) The preparation of a urease-driven Janus motor and (ii) motion control of the Janus motors by manipulating the enzymatic activity by using inhibitor/reactivator and the motion direction of the micromotor by remote magnetic field. Reprinted with permission from ref 87. Copyright 2016 American Chemical Society.

delivery. Macrophage cell membrane has been employed to cloak Janus mesoporous silica/Au MNMs. The obtained NIR light-powered macrophage cell membrane-cloaked motor can overcome the strong Brownian effect and effectively enhance the targeted recognition of cancer cells (Figure 2b).[70]

In addition to light-powered motors, chemically catalytic bubble-driven Janus heterosilica-based MNMs are also possible. As shown in Figure 2c, Xuan et al. constructed biotin-modified Janus silica micromotors with catalytic Pt half-shells for transporting and releasing anticancer drugs. The Pt coating layer could catalytically decompose the peroxide (H_2O_2) fuel to oxygen; the O_2 bubbles further propel the movement of Janus silica particles along the Pt side.[71]

In contrast to conventional Janus MNMs, Figure 2d (i) demonstrated a mesoporous heterosilica-based hollow, spherical MNMs with reversed Janus structures. The catalytic Pt hemisphere is embedded inside a hollow cavity, and the catalytic reaction occurred inside the interior, which can

https://doi.org/10.1021/acs.chemmater.1c00192
Chem. Mater. 2021, 33, 3022−3046

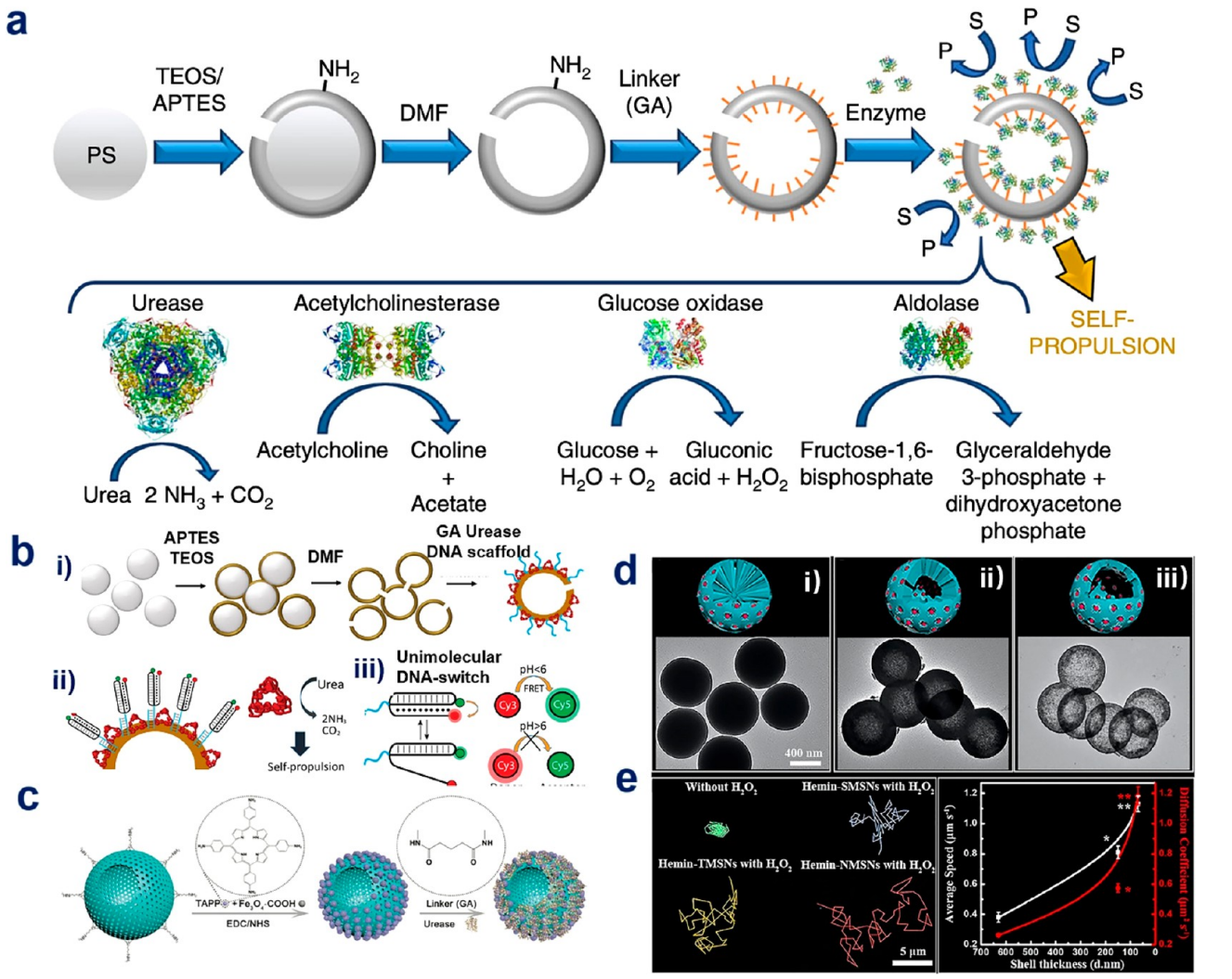

Figure 4. Spherical, hollow heterosilica-based MNMs. (a) Schematic representation of preparation of the hollow silica functionalized with enzymes. Reprinted with permission from ref 88. Copyright 2019 Springer Nature http://creativecommons.org/licenses/by/4.0/. (b) (i) Fabrication process of the micromotors, (ii) DNA micromotors and urease-triggered self-propulsion, and (iii) schematic illustration of the pH sensing strategy based on the DNA-nanoswitch, which results in a change of the FRET efficiency. Reprinted with permission from ref 91. Copyright 2019 American Chemical Society. (c) Fabrication of urease-propelled magnetic micromotors. Reprinted with permission from ref 92. Copyright 2019 Wiley-VCH. (d) TEM images show hemin-loaded mesoporous silica nanomotors: (i) mesoporous solid silica nanomotors, (ii) hollow MSNs with the shell thicknesses of 150 nm, and (iii) hollow MSNs with the shell thicknesses of 70 nm. (e) Tracking trajectories of hollow nanomotors with different shell thicknesses (left) and the average speed and diffusion coefficient of hollow nanomotors with different shell thicknesses (right). Reprinted with permission from ref 81. Copyright 2019 Elsevier Inc.

achieve self-propulsion by decomposing peroxide. Polystyrene (PS) particles with different sizes as templates, Pt, and silica were then deposited on the surface of one side via e-beam evaporation. Then a mesoporous silica layer by condensation of tetraethoxysilane (TEOS) was formed on the noncoated side of the PS sphere. Mesoporous, hollow, spherical Janus motors with different sizes ranging from 500 nm to 3 μm were obtained by dissolving PS spheres in dimethylformamide (DMF) (Figure 2d).[72] Figure 2d (ii) exhibits distinct size-dependent movement behavior: the submicron nanomotors with a size of 500 nm showed enhanced diffusion, phoretic motion toward the nonmetallic side for 1.5 and 3 μm motors. However, bubble propulsion was toward the metallic side for the 3 μm motors. Additionally, Ma et al. first reported a novel Janus motor with a mesoporous silica cluster.[73] As shown in Figure 2e, large amounts of mesoporous silica clusters are fabricated by "'unwanted'" aggregations, and a metal layer (Ni) was then deposited on one side of the mesoporous silica cluster by e-beam evaporation. Such a rough surface and narrow gap between aggregated MSNs are beneficial for bubble nucleation and growth compared to the smooth Janus surface, thus propelling the movement of motors by bubble propulsion.[48,74]

To further explore their feasibility using Janus mesoporous heterosilica-based MNMs as potential active nanocarriers for cargo delivery, Ma et al. fabricated Janus mesoporous silica nanomotors by depositing an ultrathin Pt layer (2 nm) onto the MSNs using e-beam evaporation method. A platinum catalytic layer triggered the decomposition of H_2O_2 into O_2 and H_2O, which generated a chemical gradient and further powered the movement of motors by a self-diffusiophoresis mechanism, as shown in Figure 2f.[43]

Regarding biocompatibility, enzymes represent a more suitable and versatile alternative compared with Pt catalysts

https://doi.org/10.1021/acs.chemmater.1c00192
Chem. Mater. 2021, 33, 3022−3046

for fabricating nontoxic fuel powered motors. As shown in Figure 2g, a 4 nm thin SiO_2 layer was first deposited onto one side of the mesoporous silica spheres to form a Janus structure. Enzymes were further conjugated onto the surface of the noncoated side via chemical linkage.[75] The biocatalytic mesoporous heterosilica-based MNMs are biocompatible and hold significant potential for biological applications.

2.2. Hard Template-Assisted Method. Hard templates are widely used to fabricate hollow structures; the final shape and size are essentially dependent upon the templates.[76−78] Hollow micro/nanostructures have demonstrated considerable potential in biomedical applications owing to high surface areas, large cavity volume, low density, high loading capacity, and controllable structure.[79−82] During the past decade, tremendous effort has been devoted to constructing hollow MNMs with various components including polymer, silica, metals, metal oxides, and carbonaceous materials.[12,68,81,83,84] Among these hollow MNMs available, heterosilica-based MNMs have been widely investigated as a theranostic platform for the preparation of hollow MNMs. Compared to other materials, silica was reported to be biocompatible and controllable in size in the nano/microrange. In addition, the surface chemistry of silica has been well understood, which is beneficial to further chemical modifications.[62,85] Up until now, hollow heterosilica-based MNMs with various geometric morphologies have been widely fabricated including spherical hollow motors, Janus-type hollow motors, tubular motors, etc. These synthesized hollow MNMs demonstrate great potential in biomedical applications.

2.2.1. Janus, Hollow Heterosilica-Based MNMs. Biocatalytic MNMs are emerging as a very promising tool in the biomedical field. The enzyme-triggered MNMs can be powered by the biocatalytic reaction of enzymes by anchoring biocompatible enzymes onto the surface of nanoparticles. Enzyme-powered MNMs demonstrate a more biocompatible and versatile alternative compared with inorganic catalysts engines. In addition, enzymes produce enhanced diffusion in the corresponding solution of substrates. Nevertheless, the integration of enzymes and hollow, mesoporous Janus silica structures gives a novel type of enzyme-powered motors, which are believed to be a promising direction for use in future biomedical applications.

As shown in Figure 3a, Ma et al. recently designed enzyme-powered fully biocompatible hollow mesoporous Janus nanomotors. Catalase, glucose oxidase (GOx), and urease can each be used to trigger movement of motors by the asymmetric enzymatic reaction.[86] Solid silica nanoparticles as templates were first synthesized by the classic Stöber method and further coated with a mesoporous silica shell by surfactant-induced self-assembly method. The solid silica core was then removed in Na_2CO_3 solution, yielding hollow mesoporous structures (Figure 3a (i). In order to construct an asymmetric Janus motors, hollow nanoparticles with a half-shell (10 nm SiO_2) layer were obtained using e-beam deposition as elaborated in section 2 (Figure 3a (ii). Three different enzymes (catalase, urease, and glucose oxidase (GOx)) were separately covalently conjugated onto the noncoated side by using glutaraldehyde (GA) as linker. Each enzyme can provide self-propulsion for the nanomotors by a chemophoretic mechanism generated by asymmetric reaction products. For each of these three different enzyme-modified motors, the diffusion coefficient enhanced as the fuel concentration increased (Figure 3a (iii)). They further evaluated the cytotoxicity of the obtained hollow mesoporous silica motors and the fuel urea by means of the (3-(4,5-dimethylthiazol-2-yl)-2,5-diphenyltetrazolium bromide) (MTT) assay, which demonstrated a nontoxic effect toward HeLa cells.

Motion control over both velocity and direction provides a crucial tool for controllable drug delivery. Recently, they further designed a new type of urease-powered hollow hybrid Janus motor with controlled speed and direction (Figure 3b (i)). The enzyme activity can be manipulated by adding inhibitor (Ag^+/Hg^{2+}) or reactivator (dithiothreitol), which led to different mechanical power output and thus realized an instant "on−off" switch. Furthermore, the incorporation of magnetic element within the hollow Janus silica motors achieved remote control on the movement direction (Figure 3b (ii)).[87]

2.2.2. Spherical, Hollow Heterosilica-Based MNMs. Typically, a geometrical asymmetry is required (e.g., Janus particles) to achieve an asymmetrical generation of forces, which is crucial for the movement of motors. However, some reports have proved that spherical motors can also generate a net force to move by an unbalanced distribution of enzymes. As shown in Figure 4a, Samuel and co-workers fabricated enzymatic hollow silica micromotors and systematically studied the capacity of four different enzyme to power active movement.[88] Polystyrene (PS, 2 μm) particles were first used as starting templates to coat a layer of silica shell, followed by the removal of the PS core by dimethylformamide (DMF). The obtained hollow silica microcapsules are modified with four enzymes (urease (UR), acetylcholinesterase (AChE), glucose oxidase (GOx), or aldolase (ALS) by using glutaraldehyde (GA) as a linker to study each enzyme-powered active motion. Due to the different surface roughness of silica, enzymes were nonhomogeneously distributed on the silica surface, and thus generating the asymmetric distribution of reaction products required for self-propulsion.

In order to achieve anticancer drug delivery, enzymatic nanomotors comprised of a solid silica core and a mesoporous silica shell were fabricated. The urease enzymes were anchored onto a silica shell. The mesoporous silica shell also provided a high loading capacity for anticancer drug doxorubicin (DOX). DOX-loaded urease-powered nanomotors showed an enhanced anticancer efficiency toward HeLa cells.[89] Recently, urease-powered mesoporous silica nanomotors surface functionated with antibodies have illustrated improved targeted bladder cancer therapy and diagnosis.[90]

Despite the efficiency of enzyme-powered MNMs for potential applications, it is still in its nascent stages. While most studies focused on the underlying mechanism of enzyme-powered MNMs, it is crucial to maintain enzymatic activity for the propulsion efficiency of the enzymatic MNMs. Enzymatic activity is considerably sensitive to MNMs' surrounding microenvironment change, which may lead to a different velocity of movement. Patino et al. recently demonstrated a biocompatible hollow silica enzymatic micromotor.[91] The fabrication procedure is the same as the hard-template method as mentioned above (Figure 4b (i)). Furthermore, the obtained enzymatic micromotors were anchored with a pH-responsive DNA nanoswitch (Figure 4b (ii)). Such MNMs with DNA-based nanoswitches not only can sense the micromotors' surrounding microenvironment but also provide feedback on micromotor activity status, which may be useful to further monitor their performance in different media (Figure 4b (iii)).

https://doi.org/10.1021/acs.chemmater.1c00192
Chem. Mater. 2021, 33, 3022−3046

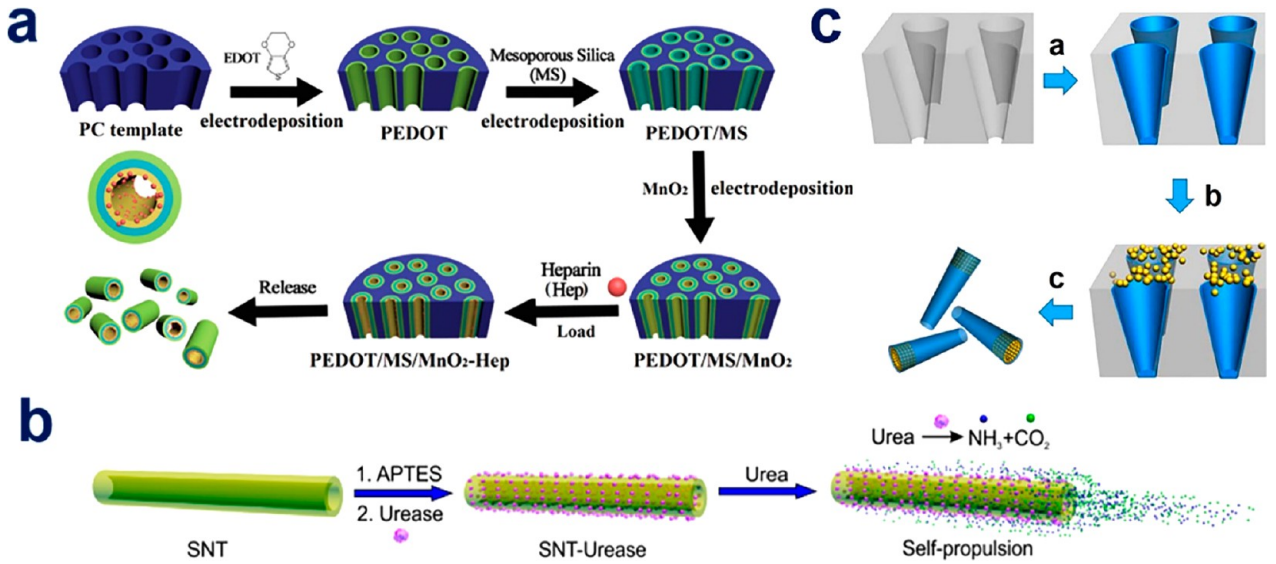

Figure 5. Schematic illustration of the preparation tubelike or wirelike heterosilica-based MNMs: (a) mesoporous tubular MNMs composed of poly(3,4-ethylenedioxythiophene) (PEDOT), mesoporous silica (MS), and manganese dioxide (MnO_2). Reprinted with permission from ref 93. Copyright 2019 The Royal Society of Chemistry. (b) Urease-driven silica tubular nanojets. Reprinted with permission from ref 94. Copyright 2016 American Chemical Society. (c) Fabrication process of the gold layer-functionalized silica tubes. Reprinted with permission from ref 95. Copyright 2017 Springer Nature http://creativecommons.org/licenses/by/4.0/.

To date, the cancer treatment is still heavily dependent on the use of anticancer drugs, and the use of many anticancer drugs is limited by dose-limiting toxicities. Photodynamic therapy (PDT) is also an effective alternative to kill cells or bacterial by transferring energy from light-excited photosensitizer to oxygen molecules ($^3O_2$) to produce cytotoxic singlet oxygen ($^1O_2$). The PDT efficiency is often reduced by the availability of $^3O_2$ molecules near photosensitizers and the extremely short diffusion range of $^1O_2$. Xu et al. envisioned self-propelled micromotors for achieving a highly efficient PDT process. They first constructed a hollow, mesoporous, enzymatic, magnetic micromotor by template-assisted method. Furthermore, 5,10,15,20-tetrakis(4-aminophenyl) porphyrin (TAPP), as a photosensitizer, was loaded onto the surface of the micromotors. The micromotors were propelled by ionic diffusiophoresis induced by the enzymatic decomposition of urea. These self-propelled MNMs serve as a mobile photosensitizer platform, significantly improving the availability of $^3O_2$ and enlarge the diffusion range of $^1O_2$ (Figure 4c).[92] Recently, based on a similar idea, Lian et al. designed hollow hemin-loaded mesoporous heterosilica-based MNMs as movable reactive oxygen scavengers to remove excess reactive oxygen species (ROS).[81] As shown in Figure 4d, mesoporous silica spheres were first synthesized by a surfactant-assembly sol−gel process. After that, the as-synthesized silica spheres were etched selectively by incubating in pure water at different temperatures. Three types of MSNs with varied shell thicknesses (solid, thick-walled, and narrow-walled) were obtained, and hemin is evenly loaded on the mesoporous shell. The obtained nanostructures were propelled by harnessing chemical free energy from the catalytic reaction. Figure 4e displays tracking trajectories of hemin-loaded nanomotors with different shell thicknesses in the presence of 30 mM H_2O_2. The average speed of narrow-walled hollow nanomotors was 3.5 times higher than that of solid nanomotors. By virtue of active self-propulsion, hemin-loaded mesoporous silica MNMs demonstrated higher ROS scavenging ability compared to free hemin molecules. Such a movable ROS provides a new possibility for the application of mesoporous silica MNMs in the biomedical field.

2.2.3. Tubelike and Wirelike Heterosilica-Based MNMs. Hard template-assisted method is one of the most common means to synthesize tubular MNMs. The final structures synthesized by this method have significant advantages including well-defined morphology, uniform size, and good monodispersity. At present, conductive polymer materials, such as polyaniline (PANI), poly(3,4-ethylenedioxythiophene) (PEDOT), and polypyrrole (PPy), have been used to prepare tubular MNMs. However, polymer-based tubular MNMs usually require further surface modification for drug loading, which leads to low loading capacity onto the surface of tubular MNMs. Mesoporous silica, due to exceptionally large surface areas, an ordered mesoporous structure, and a high loading capacity, has been widely used to prepare MNMs with different morphologies such as Janus motors, spiral motors, and hollow motors as mentioned above. It has been reported that MNMs with linear structures (e.g., tubular motors and spiral motors) have longer circulation times in the blood.

Wang et al. designed a mesoporous tubular MNMs composed of poly(3,4-ethylenedioxythiophene) (PEDOT), mesoporous silica (MS), and manganese dioxide (MnO_2) by template-assisted electrochemical deposition.[93] As shown in Figure 5a, the obtained PC membrane has a 5 mm pore diameter as the starting template, followed by deposition of a PEDOT layer, mesoporous silica, and a MnO_2 layer in sequence. The PEDOT layer was removed by calcination and thus observed the mesoporous structure of the silica layer. Then, heparin was loaded into mesoporous silica via a simple soaking method. Finally, the mesoporous tubular micromotors were released. The tubular MNMs were propelled by O_2 bubbles from the decomposition of H_2O_2 fuel catalyzed by MnO_2, which presented an effective loading capacity and controlled release. Until now, the diameter of most tubular MNMs reported is from submicrometer up to 30 μm.

https://doi.org/10.1021/acs.chemmater.1c00192
Chem. Mater. 2021, 33, 3022−3046

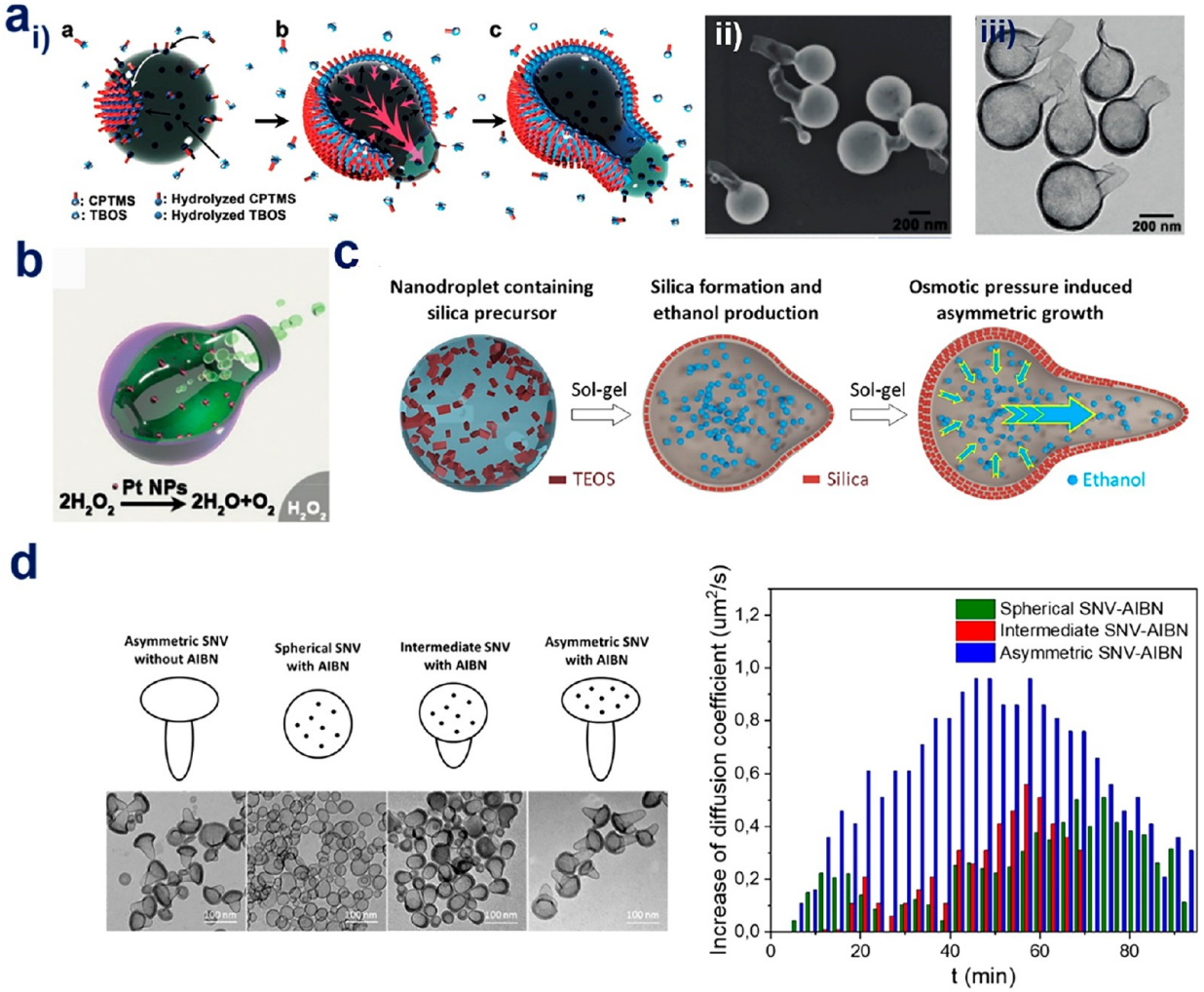

Figure 6. (a) (i) Illustration of the formation of silica nanobottles, (ii) SEM images, and (iii) TEM images of the silica nanobottles. (b) Self-propelling silica nanobottles. Reprinted with permission from ref 96. Copyright 2016 Wiley-VCH Verlag. (c) Schematic illustration of the preparation of asymmetric silica nanovehicles. (d) TEM images of silica nanovehicles with different degrees of asymmetry (left) and the corresponding diffusion coefficient in the absence of fuel (right). Reprinted with permission from ref 7. Copyright 2019 American Chemical Society.

However, recent research has proved that the carriers with diameters of ∼200 nm achieved a longer circulation time in living organisms, thus reducing the possibility of drugs being cleared by the immune system.

Ma et al. fabricated ultrasmall (220 nm diameter on average) bubble-free propelled tubular silica nanomotors by the silver nanowire-assisted method.[94] First, silver nanowires with a width of ∼115 nm and a length of 50 μm were used as a template to grow a thin layer of silica by the sol−gel method. The obtained silica-coated silver nanowires were further broken down into shorter segments by sonication, followed by removal of the silver templates by etching. Then the final silica tubular nanojets were modified with the enzyme urease, and an internal flow formed inside the tube extends through the opening in the external fluid by an enzyme-triggered biocatalysis, leading the self-propulsion (Figure 5b). The tubular nanojets have great advantages such as nanosized diameter, longitudinal self-propulsion, and good biocompatibility, which is possible for future in vivo biomedical use.

For tubular motors, besides catalytic reaction-triggered self-propulsion, a fuel-free, near-infrared light-powered tubular micromotors were designed by He's group.[95] As demonstrated in Figure 5c, a porous membrane was first used as a template and multilayer silica was deposited inside the pores by the layer-by-layer sol−gel process, followed by the assembly of gold clusters in the large opening of the pores. Under the irradiation of NIR light, the Au-functionalized silica tubes generate a thermal gradient inside the tube owning to the photothermal effect of the gold layer, which propels the movement of the tube by the self-thermophoretic mechanism.

2.3. Interfacial Self-Assembly Strategies for Hetero-silica-Based Asymmetric Structures. Interfacial assembly strategy has been extensively applied in designing various complex asymmetric architectures due to its great flexibility in component control, structural design, and functionalization. In this section, different methods based on interfacial assembly mainly including conventional emulsion-induced growth, Pickering emulsion-based growth, and emulsion-oriented interfacial epitaxial self-assembly are discussed for the fabrication of heterosilica-based MNMs. Moreover, interface-energy-mediated assembly can be introduced for the fabrication of multifunction, asymmetric, mesoporous architectures. These interfacial self-assembly strategies have provided a promising platform for the construction of new

https://doi.org/10.1021/acs.chemmater.1c00192
Chem. Mater. 2021, 33, 3022−3046

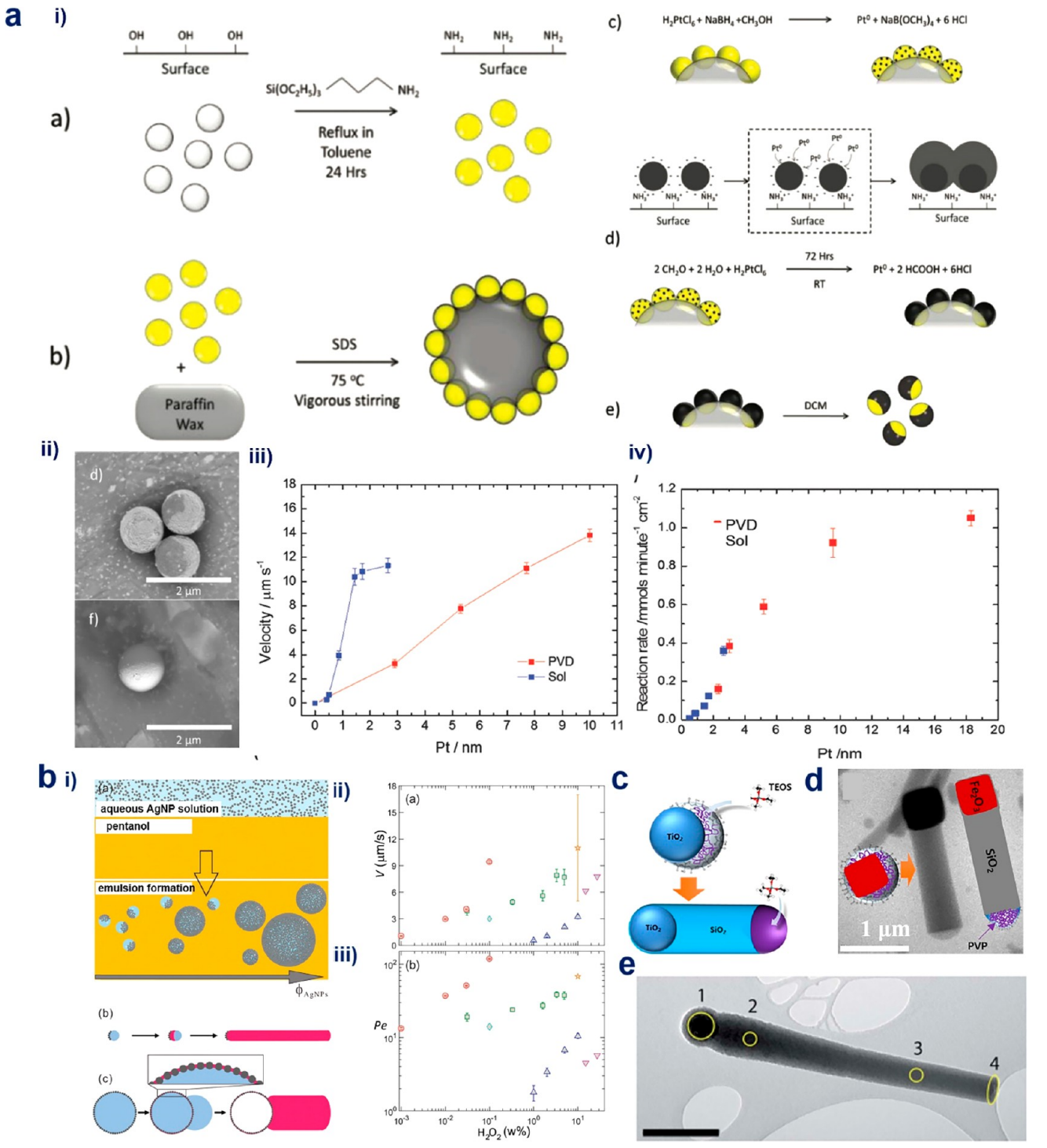

Figure 7. (a) (i) Schematic showing the formation mechanism of active Pt-SiO_2 Janus colloids by solution synthesis. (ii) Backscattered electron images of Pt-silica Janus motors prepared by Pickering emulsion method (top) and PVD (bottom). (iii) Translational velocity and (iv) reaction rate of decomposition of H_2O_2 per colloid active surface area of active colloids prepared in solution and by PVD. Reprinted with permission from ref 48. Copyright 2017 Wiley-VCH Verlag https://creativecommons.org/licenses/by/4.0/. (b) (i) Schematics illustration of the preparation of silver-silica rod growth, (ii) self-propelled velocity, and (iii) the corresponding Peclet number as a function of the H_2O_2 fuel concentration for different samples. Reprinted with permission from ref 99. Copyright 2018 The Royal Society of Chemistry. (c) Schematic showing the mechanism of formation silica-MnO_2 and (d) the TEM images of silica-Fe_3O_4 "matchstick". Reprinted with permission from ref 100. Copyright 2018 American Chemical Society. (e) Silica-TiO_2 "matchstick" shaped motors. Reprinted with permission from ref 101. Copyright 2014 The Royal Society of Chemistry.

family of nanocarriers with tunable pore parameters, surface topology, morphologies, and functions, showing great potential for use in the further development of heterosilica-based MNMs.

https://doi.org/10.1021/acs.chemmater.1c00192
Chem. Mater. 2021, 33, 3022−3046

2.3.1. Interfacial Self-Assembly by Conventional Emulsion-Induced Growth. Emulsions can always be formed by mixing two or more immiscible solvents with the assistance of external forces. They can be divided into oil-in-water emulsions and water-in-water emulsions with typical sizes ranging from 10 to 100 nm. Generally, the formed emulsions are unstable because a phase separation process is always active, so a certain amount of surfactants are usually employed to act as stabilizing agents to form thermodynamically stable microemulsions. Apart from the surfactant-based emulsions, Pickering emulsion is also an attractive formulation, which is an emulsion stabilized by solid particles.

Wang et al. designed bottlelike nanomotors by anisotropic sol−gel growth in a water/*n*-pentanol emulsion as shown in Figure 6a.[96] A water/oil emulsion is first formed, and the (3-chloropropyl) trimethoxysilane (CPTMS) and tetrabutylorthosilicate (TBOS) are used as a silica precursor. The CPTMS molecules hydrolyze into a hydrophilic head and hydrophobic tail when meeting the formed water droplet. The hydrophilic component inserts into the water droplet while the hydrophobic end remains in *n*-pentanol, thus forming a thin silica shell on the droplet surface. TBOT in the oil phase hydrolyzes and migrates into the water droplet, further condensing at the formed silica shell. By continuous deposition of hydrolyzed TBOT, aqueous solution is gradually extruded out of the droplet to produce a new water−oil interface. The co-condensation of hydrolyzed CPTMS and TBOS at the newly formed water−oil interface finally produces a silica nanobottle with an opening. SEM and TEM images of the silica nanobottle are shown in Figure 6a (ii and (iii). In order to propel the movement of a silica nanobottle by catalytic reaction, hydrophilic Pt nanoparticles were selectively loaded inside the nanobottle. The obtained silica bottle-like nanomotors can be self-propelled by O_2 bubbles produced by Pt catalytic decomposition of H_2O_2 (Figure 6b).

Compared to the postencapsulation method, a simple one-step coassembly was reported by Jiang et al. to prepare fuel-containing asymmetric silica nanocapsules with a diameter of ∼100 nm.[7] As shown in Figure 6c, an oil-in-water miniemulsion containing energy molecules (AIBN) was first synthesized through a microfluidization process, the tetraethyl orthosilicate (TEOS) in the oil phase was hydrolyzed and condensed on the oil−water interface, and a silica shell was hence formed. During this step, hydrolysis of TEOS produced a significant amount of ethanol, which leads to the osmotic pressure and therefore drives the anisotropic growth of the nanocapsules. The obtained silica nanovehicles with internally stored AIBN fuels can be activated to release nitrogen gas under heat or light irradiation. Due to the very thin silica layer at the end of the tail, the generated nitrogen gas can escape easily from the cavity of the nanocapsule and further propel the movement of the nanocapsules. It is usually difficult to directly characterize small nanocapsules with a diameter of only ∼100 nm by optical microscopy, so the self-propulsion is characterized by enhanced diffusion. The silica nanocapsules showed higher diffusion coefficient than its equilibrium value by dynamic light scattering. Furthermore, Jiang et al. investigated the correlation between nanovehicle morphology and their diffusion coefficient. As shown in Figure 6d, an asymmetric nanocapsule with a higher asymmetric degree demonstrated the highest diffusion coefficient compared with the nanocapsule with a spherical shape or a lower degree of asymmetry. It has been found that the drag coefficient of MNMs significantly reduced as an increased ratio of length to radius.[97] These results indicate that asymmetric geometry with a higher asymmetric degree is beneficial for achieving effective self-propulsion.

MNMs have been extensively explored but it remains an intriguing challenge for their measurement. MNMs usually move in three-dimension space, even in very thin fluid layers. The movement features along the *Z*-axis direction cannot be quantified by current means of characterization. On the other hand, most studies have focused on MNMs larger than 300 nm in size while the motors on the nanometer scale is missing. It has recently been proposed that nanoparticles with sizes smaller than 100 nm may play a role for further molecular transport at the cellular lever. It is therefore significant to further explore their self-propulsion behavior at the nanoscale. However, the smaller the length scale, the more dominant randomizing Brownian forces become, making direct characterization of their velocities experimentally challenging. Therefore, it is necessary to explore other suitable devices that can measure their motion behavior more accurately.

2.3.2. Interfacial Self-Assembly by Pickering Emulsion-Based Growth. Apart from conventional surfactant-based oil-in-water emulsions or water-in-oil emulsions, special emulsion systems such as Pickering emulsions are also employed for the purpose of asymmetric hybrid heterosilica-based MNMs. The synthesis processes of the Pickering emulsion are similar to the procedures for the normal emulsion templating method except with solid particles being used as stabilizers. The advantage is that it generally provides a more stable system than surfactant-stabilized emulsions. Moreover, the template can easily be removed by evaporation.[98]

Archer et al. fabricated SiO_2/Pt Janus particles by Pickering emulsion masking combined with solution phase metallization.[48] As was stated in section 2, the synthesis of Janus MNMS at present relies on the PVD process, which is difficult to scale up and requires expensive equipment.[44] Picking emulsion method is an alternative manufacturing route to produce Janus particles in bulk quantities. Figure 7a (i) demonstrated the process of SiO_2/Pt Janus particles. The silica colloids were first prepared and functionalized with amine groups. In order to mask one side, the functionalized silica spheres were added into stable wax-in-water emulsions and trapped at the oil/water interface. The exposed area was chemically modified with platinum, via two-stage seeding and growth reactions. After completing platinum growth, the masking wax is dissolved and finally obtained freed SiO_2/Pt Janus colloids.

In order to assess their motion performance, Archer et al. also synthesized SiO_2/Pt Janus particles by the conventional PVD technique. Figure 7a (ii) shows backscattered SEM images with different surface roughness of the platinum coating. The Janus colloids prepared by chemical reduction of platinum precursors show higher surface roughness than Janus particles prepared by PVD. They further compared catalytic activity of H_2O_2 and propulsion velocity for the Janus particles prepared by different methods. Figure 7a (iii) shows that the solution prepared colloids show higher translational velocity at thinner Pt thickness than PVD prepared colloids. It is noted that solution and PVD-based Janus particles show a similar reaction rate for decomposition of H_2O_2 per area, see Figure 7a (iv). These results suggested that the rougher surface may increase the propulsion velocity, which is not linked to fuel decomposition rate. More importantly, less Pt is required

https://doi.org/10.1021/acs.chemmater.1c00192
Chem. Mater. 2021, 33, 3022−3046

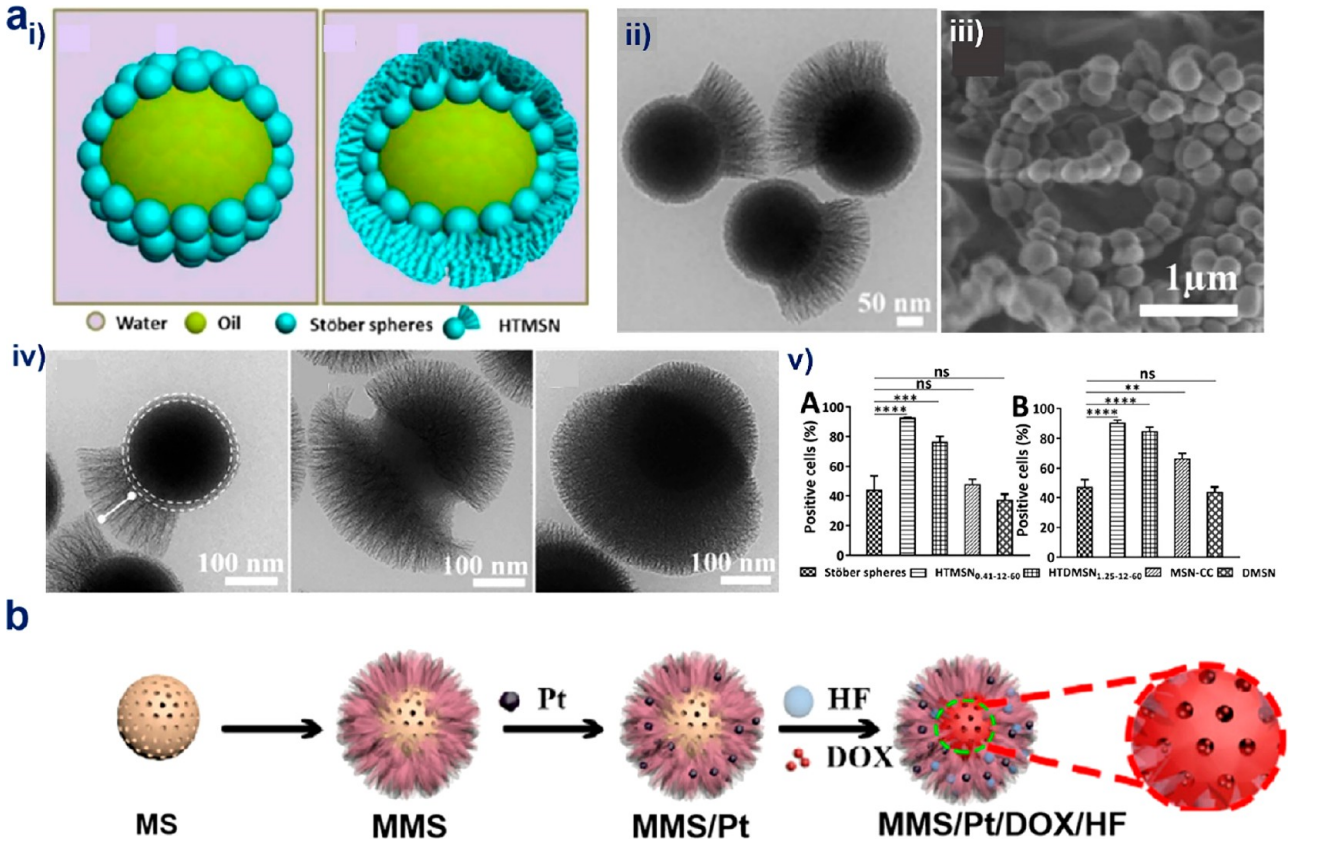

Figure 8. (a) (i) Schematic illustration of a droplet stabilized by silica spheres (left) and the further orientation of dendritic silica tail growth (right). (ii and iii) TEM and SEM images of head−tail MSNs. (iv) TEM images of head−tail structures prepared at varied TEOS volumes. (v) Cellular uptake efficiency of three nanoparticles. Reprinted with permission from ref 102. Copyright 2017 American Chemical Society. (b) Schematic illustration of the formation of multifunctional mesoporous-microporous silica/Pt/DOX/HF nanomotors for targeted cancer therapy. Reprinted with permission from ref 103. Copyright 2020 Wiley-VCH Verlag.

to produce rapid propulsion by Pickering emulsion masking method, which could open a pathway for cheaper synthesis approaches for catalytic MNMs.

The Pickering emulsion approach is also usually used to fabricate other asymmetric hybrid structures. For instance, Gao et al. prepared a hollow silver-head colloidal silica rods nanomotors by the simple wet-chemistry method.[99] The synthesis mechanism is based on the formation of Pickering emulsions stabilized by photoactive silver particles (AgNPs) and directional growth of silica rodlike particles. First, AgNPs solution with different concentrations was mixed with pentanol to form emulsions. The higher the concentration of silver nanoparticles solution, the more silver particles covered the water droplets, until the water droplets were fully covered. At intermediate concentrations, the AgNPs partially covered the water droplets. The AgNPs served as the initial nucleation sites for precipitation of silica, the water droplets will be pushed to the opposite end of AgNPs as continuous deposition of silica and finally obtained directional growth of silica rod along the opposite side of AgNPs. Therefore, hybrid asymmetric silica MNMs with solid or hollow silver-enriched head were fabricated under the conditions of partially and fully covered droplets, respectively, see Figure 7b (i). The active silver head reacts with hydrogen peroxide, leading to asymmetric release of O_2 and Ag^+ and HOO^- ions. Due to different diffusion rates, a local electric field pointing toward the end of the silver head is generated. As a result, the obtained asymmetric Ag-silica nanomotors show self-propulsion based on an electrolyte self-diffusiophoresis mechanism. Furthermore, Gao et al. compared the self-propulsion performance of hollow Ag-silica rods to existing Pt-based MNMs including to-date most motile Pt-based MNMs. As shown in Figure 7b (ii), it is clear that the hollow Ag-silica rods displayed similar velocity as other MNMs but operated at very low fuel concentrations. Even compared to the to-date most motile Pt-based MNMs, hollow Ag-silica rods still reduced the H_2O_2 concentration by 2 orders of magnitude while maintaining the same Peclet number (*Pe*) (Figure 7b (iii)). The high performance may be attributed to the special morphology with the large, rough, and hollow head, which provides a large active surface area, making reaction of silver with hydrogen peroxide more active and thus enhancing self-propelled motion.[48] In addition, silica-TiO_2, silica-Fe_3O_4,[100] and silica-MnO_2[101] "matchstick" shaped motors with a catalytic head are also fabricated by the Pickering emulsion approach. These asymmetric structures can achieve catalytic self-propulsion by consumption of hydrogen peroxide (Figure 7c−e).

2.3.3. Emulsion-Oriented Interfacial Epitaxial Self-Assembly. Another typical strategy is emulsion-oriented interfacial epitaxial self-assembly for the construction of asymmetric nanostructure with bimodal mesopores.[102] As shown in Figure 8a (i−iii), solid or mesoporous silica spheres can be used to stabilize the oil-in emulsion droplets, and then nucleation and the growth direction of the tails occur preferentially toward water, leading to the formation of asymmetric head-dendritic tails with large pores structures (11−28 nm). Moreover, the

https://doi.org/10.1021/acs.chemmater.1c00192
Chem. Mater. 2021, 33, 3022−3046

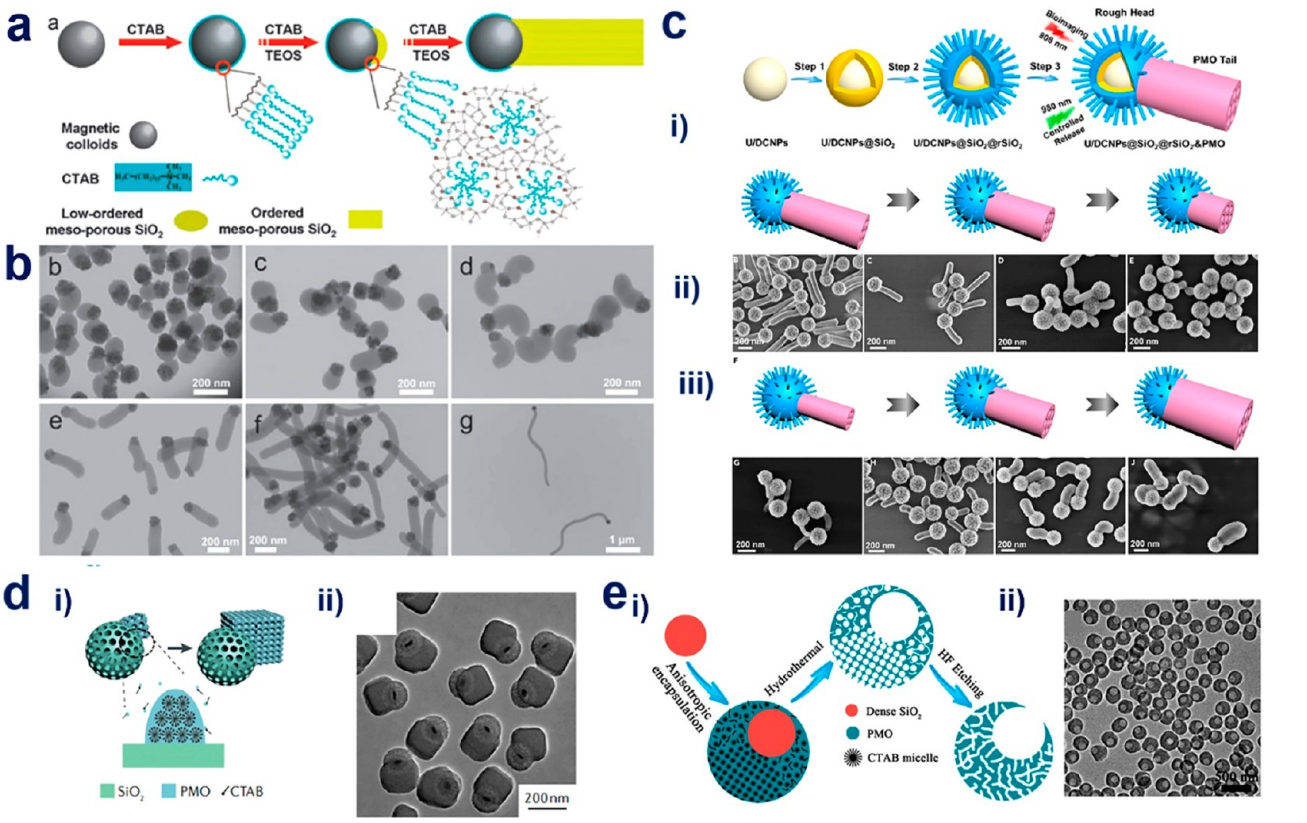

Figure 9. Interfacial energy-mediated interfacial self-assembly growth for the preparation of mesoporous heterosilica-based symmetric multifunctional architectures. (a) Scheme illustrations of the preparation of Fe_3O_4−SiO_2 Janus particles and (b) TEM images of Fe_3O_4−SiO_2 Janus particles with different aspect ratios. Reprinted with permission from ref 108. Copyright 2011 The Royal Society of Chemistry. (c) (i) Synthetic procedure of the nanotrucks, (ii) SEM images of nanotrucks with different lengths of PMO domains, and (iii) nanotrucks with different diameters of PMO domains. Reprinted with permission from ref 107. Copyright 2020 Elsevier Inc. (d) (i) Schematic of mesoporous SiO_2/PMO Janus nanoparticles and (ii) TEM image of these nanoparticles. Reprinted with permission from ref 25. Copyright 2014 American Chemical Society. (e) (i) Fabrication procedure of the asymmetric single-hole mesoporous nanocages and (ii) TEM images of the obtained nanocages. Reprinted with permission from ref 82. Copyright 2015 American Chemical Society.

dendritic mesoporous tail length and tail coverage on head particles are adjustable by changing TEOS amount. As shown in Figure 8a (iv), TEM images clearly show that the particle size and tail coverage increased with increased TEOS amount. The head−tail structures with viruslike surface topology show enhanced cellular uptake (Figure 8a (v)). Such sophisticated structures with hierarchical pore geometry (mesoporous-microporous) hold significant potential for biological applications. Very recently, Wan et al. used such asymmetric structures with hierarchical pores to design a NIR-driven multidrug loaded silica/Pt nanomotors for cancer chemo/photothermal therapy. DOX and new targeted anticancer drug heparin-folate (HF) nanoparticles with a larger size (20−40 nm) were loaded into mesopores and macropores, respectively. The Pt nanoparticles with 20−40 nm are asymmetrically loaded in microporous silica and generated a thermal gradient due to their unique surface plasmon resonance effect (SPR) under NIR irradiation to propel the nanomotors. Such multifunctional nanomotors with viruslike surface topology enhance tissue permeability of drugs, allowing for targeted drug delivery into cancer cells (Figure 8b).[103] Furthermore, they used the same silica/Pt structures to load large-sized thrombolytic drug of urokinase (UK) and anticoagulant drug of Hep (heparin), and the platelet membrane (PM) was then coated on the surface of the motors for targeted release at the thrombus site.[104] The integration of the targeting ability and active motion ability show effective thrombus therapy.

2.3.4. Interfacial Self-Assembly by Interfacial Energy-Mediated Growth. In nanosynthesis, the interfacial energy is often the key contributing factor in engineering chemical compositions, morphologies, and sizes.[105] Interface-energy-mediated anisotropic growth is another interfacial self-assembly approach, which can produce asymmetry in geometry, chemical composition, surface property, and functionality in a controllable, low-cost, and mass-produced manner. The anisotropic growth is mainly dependent on lattice mismatch between seeds and the growth material (GM), which induces the formation of disordered region of GM at the heterointerface and further growth along both the axis and radial to form the asymmetric nanostructures. During the growth process, the total surface energy variation ($\Delta\sigma$) can be represented as

$$\Delta\sigma = \sigma_{\mathrm{GM-solvent}} + \sigma_{\mathrm{GM-seed}} - \sigma_{\mathrm{seed-solvent}}$$

where $\sigma_{\mathrm{GM-solvent}}$ and $\sigma_{\mathrm{seed-solvent}}$ are the solid−liquid interfacial energies of the GM and the initial seed in the solvent, and $\sigma_{\mathrm{GM-seed}}$ is the solid−solid interfacial energy between GM and the initial seed. When $\Delta\sigma > 0$, GM often follows the Volmer−Weber growth mode to form segregated islands on the seed surface. In comparison, when $\Delta\sigma < 0$, GM often epitaxially overgrow on the seed surface by the Frank−van der Merwe or

https://doi.org/10.1021/acs.chemmater.1c00192
Chem. Mater. 2021, 33, 3022−3046

FM growth mode, leading to eccentric core@shell structures.[106,107]

In this method, the surfactants usually are used to as a mesoscaled template to form ordered mesoporous materials. They can organize into surfactant-oligomers micelles with organic or inorganic oligomers at their critical micelle concentration (CMC) due to their hydrophilic and hydrophobic components, the formed micelles soft template is easy to remove.[25] Up until now, a variety of multifunctional asymmetric heterosilica-based nanomaterials with ordered mesoporous structures have been prepared through interfacial self-assembly strategy. These multifunctional materials are very suitable as MNMs for biomedical applications.

For example, Zhang et al. reported mesoporous Fe_3O_4−SiO_2 head−tail structures with a tunable aspect-ratio and excellent magnetic properties by the interface-energy-mediated assembly method (Figure 9a).[108] The interface energy can be tuned by varying the polarity of the reaction solvent; under the water-based reaction conditions, anisotropic nucleation and growth of the CTAB/silicate micelles were achieved, which led to rodlike silica. In contrast, only a core−shell structure of Fe_3O_4@silica was obtained when reaction is performed in either a water−ethanol mixture or ethanol solution due to the low interface energy between Fe_3O_4 and SiO_2. In this approach, the aspect ratio of obtained Janus nanoparticles can be precisely tuned in the range from hundreds of nanometers to a few micrometers by changing the molar ratio of TEOS/Fe_3O_4 (Figure 9b). Such multicomponent mesoporous Janus nanoparticles demonstrate an efficient response to external magnetic stimuli, which holds enormous potential for targeted therapy in cancer. The Fe_3O_4 core nanoparticles in the head region can be used for external magnetic guidance of the motor' movement.

Zhao group designed a multifunctional dual-compartment asymmetric nanotruck composed of viruslike UCPN@SiO_2 nanospheres (UCNP, upconversion nanoparticle) with a rough surface and a periodic mesoporous organosilica (PMO) nanorod (Figure 9c).[107] The viruslike rough surface morphology was first prepared through a single-micelle epitaxial growth in a low-concentration surfactant biphase system reported by the same group. The viruslike head as an "engine" could effectively penetrate the cellular membrane and achieve rapid internalization during the invasion process. The rodlike PMO tails with a high surface area were anisotropically assembled on the head with a rough surface by the interface-energy-mediated growth strategy for efficient drug loading in Figure 9c (i). Moreover, it was found that the lengths (80−560 nm) and diameters (60−230 nm) of the PMO nanorods on the rough surface can be well controlled by simply tuning the initial amount of SiO_2 nanoparticles with the rough surface and concentration of the PMO procurers, respectively, which in turn increase the drug loading capacity (Figure 9c (ii and iii).

It is also possible to synthesize asymmetric nanostructures with different pore sizes via the interfacial assembly method. Here multifunctional Janus nanocomposites of UCNP@SiO_2@ mesoporous SiO_2 nanospheres and PMO nanocubes with ordered dual independent mesopores of 2.1 and 3.5 nm are prepared by the Zhao group (Figure 9d).[25,65] The ultimate asymmetric architectures are mainly affected by the volume ratio of H_2O/ethanol. When the volume ratio of H_2O/ethanol is high (∼15:1), the interfacial energy between PMO and solvent increase and the interfacial energy is low between SiO_2 and PMO. It means that it is not easy for the CTAB-organosilica micelles to spread on the SiO_2 surface. Hence, the energy barrier results in the island nucleation and growth of the initial PMO nucleus (Figure 9d (i)). The obtained asymmetric Janus nanostructures possess highly uniform sizes of ∼300 nm and a large surface area of ∼1290 m^2/g (Figure 9d (ii)). The unique Janus mesoporous silica nanocomposites with bimodal pore sizes can be used for loading of multiple guests, achieving controllable release of dual-drugs.

Another interesting structure is exploited by the same group. They reported an asymmetric mesoporous silica shell with a hole on their surface.[82] The dense SiO_2 nanospheres were first prepared as initial seeds, PMO was then anisotropically nucleated and encapsulated on the surface of SiO_2 seeds to form asymmetric Janus nanostructure by controlling the interfacial energy, followed by the etching of dense SiO_2 nanospheres via hydrothermal treatment, and the eccentric hollow nanostructures were obtained. Finally, it is required to use HF solution to further etch the thinner side of the PMO shell to form the nanocages with an open hole (Figure 9e (i)). Such nanocagelike structures possess uniform mesopores (2−10 nm) and a large void (∼25 nm), which endows them with excellent dual-sized guests loading capacity including small molecules and large molecules or nanoparticles (Figure 9e (ii)). The large void could be potentially used for loading nanoparticles (∼20 nm) with the SPR effect (e.g., Pt), which can exert a thermal gradient across the nanocages due to the photothermal effect of Pt under NIR irradiation to propel the movement of MNMs. Therefore, the asymmetric, biocompatible silica nanocages with dual pore sizes could be used in drug delivery in future MNMs.

3. HETEROSILICA-BASED MNMS FOR IN VITRO AND IN VIVO APPLICATIONS

Over the past decade, a variety of self-propelled MNMs have been designed for biomedical applications including targeted cargo transportation, anticancer drug delivery, and cancer therapy. The active propulsion of MNMs plays a key role in efficient bioseparation and precise delivery of anticancer drugs. More works are now being carried out for practical applications in vivo and show considerable promise in the biomedical field. In this section, we outline recent significant advances of heterosilica-based MNMs in the biomedical field.

3.1. Targeted Drug Delivery. To date, it remains a significant challenge to develop specific target drug delivery systems that can achieve efficient drug encapsulation and delivery of therapeutic and diagnostic agents to the target locations controllably.[109] Generally, nanocarriers are used to load anticancer drugs and deliver them into cancer cells by endocytosis, which not only lacks sufficient penetration and targeting but also make patients resistant to chemotherapy. Therefore, such a passive delivery manner seriously affects the drug therapeutic effect. Mesoporous heterosilica-based MNMs as a powerful alternative possess outstanding drug-loading capacity and can integrate self-propulsion and navigation capability, which not only facilitate tissue penetration but also achieve on-demand encapsulation and release of drugs toward targeted biological tissues or cells.

Mesoporous heterosilica-based MNMs can transport and deliver cargoes in an active manner by self-propulsion by external stimuli or chemical fuels. Fuel-dependent MNMs usually are propelled by nonbiotoxic or biocompatible fuels. Fuel-free MNMs can be powered by external stimuli such as light, magnetic and electric fields, or ultrasonic waves.

https://doi.org/10.1021/acs.chemmater.1c00192
Chem. Mater. 2021, 33, 3022−3046

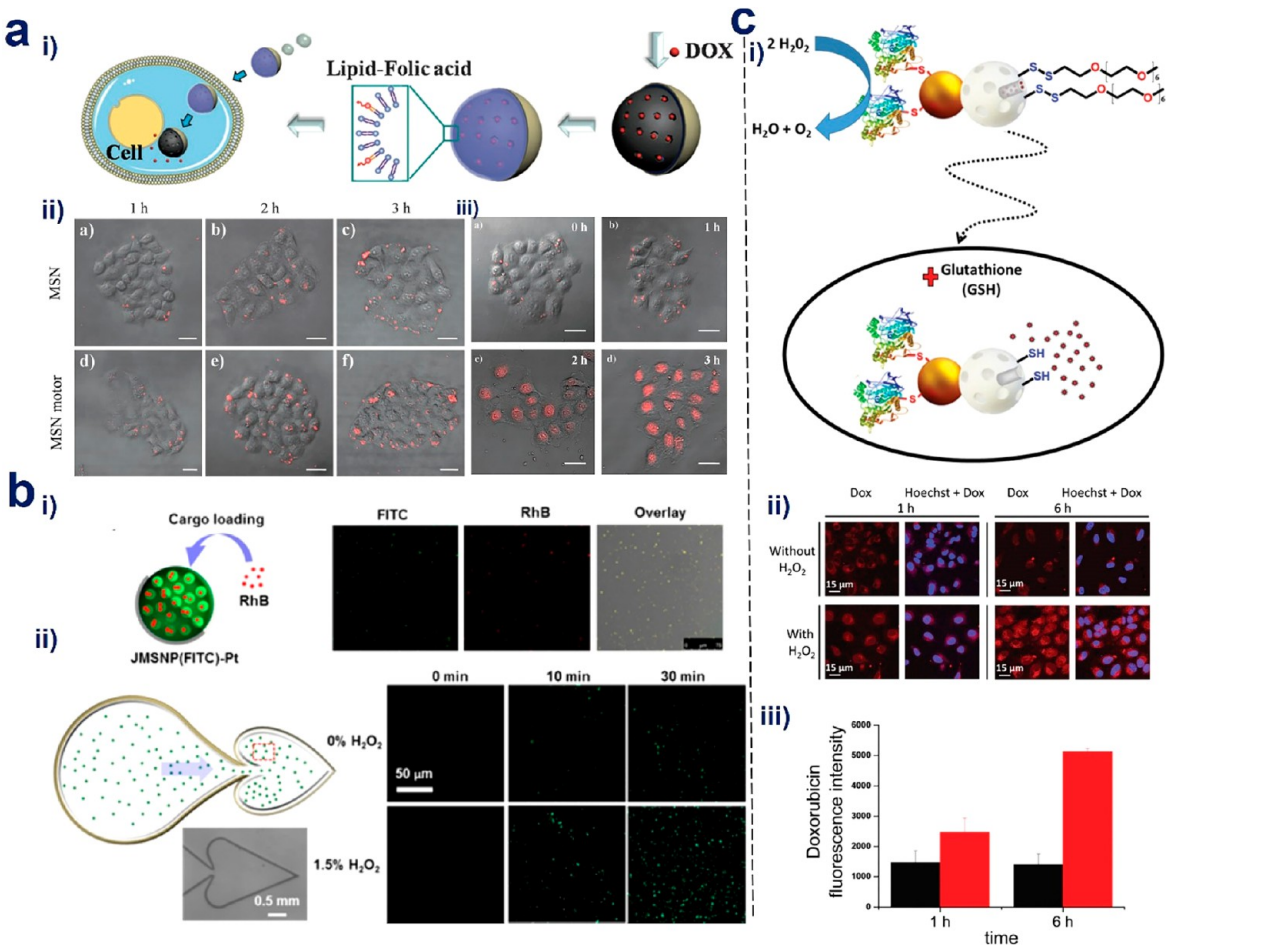

Figure 10. H_2O_2 powered heterosilica-based MNMs. (a) (i) Preparation of nanomotor and the drug loading, lipid bilayer modification, and drug release process in cells and (ii) CLSM overlay images of the fluorescence image and a differential interference contrast (DIC) image of egg PC modified mesoporous silica nanoparticles (top) and Janus nanomotors incubated with HeLa cells in the presence of 0.2% H_2O_2 (bottom). (iii) Cargo delivery from egg PC modified Janus nanomotors inside HeLa cells for different times. The images are overlays of fluorescence and DIC channels. Scale bars = 10 mm. Reprinted with permission from ref 71. Copyright 2014 Wiley-VCH Verlag. (b) (i) CLSM images of RhB loaded Janus nanomotors (scale bar is 75 μm). (ii) Schematic illustration of on-chip cargo delivery by Janus nanomotors and (iii) enhanced accumulation toward the target reservoir of active diffused Janus nanomotors. Reprinted with permission from ref 43. Copyright 2015 American Chemical Society. (c) (i) Schematic representation of the performance of enzyme-powered Janus Au-mesoporous silica and glutathione-responsive drug delivery capabilities. (ii) Confocal microscopy images of HeLa cells incubated with nanomotors for 1 and 6 h in the absence and in the presence of H_2O_2 and (iii) quantification of DOX-fluorescence in cells incubated with nanomotors in the absence (black) and in the presence of H_2O_2 (red). Reprinted with permission from ref 111. Copyright 2019 The Royal Society of Chemistry.

Depending on the types of loaded drugs, MNMs based on mesoporous silica can achieve treatment for different types of cancers, which endows them with more flexibility in cancer treatment. Therefore, the mesoporous heterosilica-based MNMs are ideal candidates as smart vehicles for drug delivery in biomedical applications.

3.1.1. H_2O_2 Powered Heterosilica-Based MNMs. One of the main challenges of nanocarrier-based drug delivery is to develop efficient delivery systems that can deliver the therapeutic agents to the target site as designed without damaging normal cells. To address the issue, MNMs with high drug loading and target delivery capabilities have been given growing attention. Self-propulsion promotes the targeting ratios by actively seeking the tumor site and provides a considerable propulsive force to penetrate the tumor beyond their ordinary diffusion limits.[110]

He's team reported a mesoporous silica nanomotor with sputtered chromium/platinum metallic caps and with a diameter of less than 100 nm.[71] Anticancer drugs were loaded into the noncoated mesoporous silica by physical adsorption and further covered with an egg phosphatidylcholine (egg PC) bilayer, which promotes adhesion to the nanomotors on the surface of tumor. They compared the drug delivery efficiency of active motors using chromium/platinum sputtered Janus nanoparticles and unsputtered mesoporous silica nanoparticles as passive carriers (Figure 10a (i)). In the presence of 0.2% H_2O_2 containing HeLa cells, more chromium/platinum capped Janus nanomotors were taken up and located in the cytoplasm of HeLa cells than unsputtered nanoparticles, exhibiting the advantage of active drug delivery (Figure 10a (ii)). In Figure 10a (iii), the images of overlays of fluorescence and DIC channels images observed DOX release from egg PC modified Janus MSN nanomotors inside HeLa cells at different times. Due to the catalytic hydrolysis of the egg PC bilayers in the Hela cells, the red area in the HeLa cells gradually became larger, which suggested that more encapsulated DOX was released into the cytoplasm. Moreover, released DOX molecules can easily enrich the nucleus HeLa cells by

https://doi.org/10.1021/acs.chemmater.1c00192
Chem. Mater. 2021, 33, 3022−3046

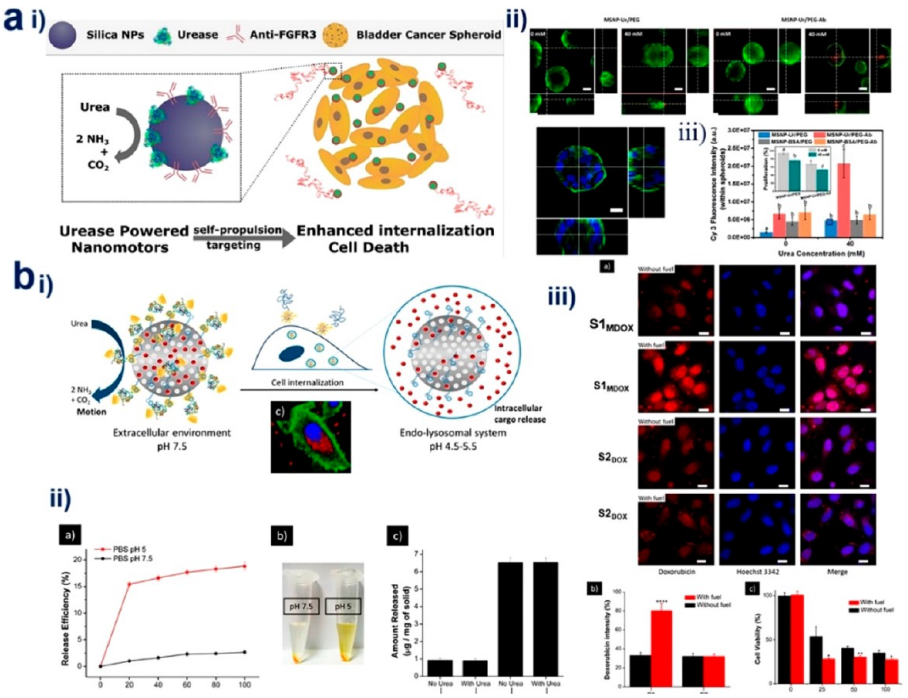

Figure 11. (a, b) Nontoxic fuel powered heterosilica-based MNMs. (a) (i) Urease-powered silica nanomotor with functionalized-anti-$FGFR_3$ on the outer surface for targeted bladder cancer therapy. (ii) Targeting abilities of anti-$FGFR_3$-modified nanomotors into 3D bladder cancer spheroids. Reprinted with permission from ref 90. Copyright 2018 American Chemical Society. (b) (i) Schematic illustration of the performance of enzyme-powered stimuli-responsive mesoporous silica nanomotors, (ii) cargo release experiments from stimuli-responsive nanomotors at physiological pH (7.5, black curve) and at lysosomal pH (5, red curve), and (iii) delivery of DOX in HeLa cells. Reprinted with permission from ref 114. Copyright 2019 American Chemical Society.

recognizing DNA chains and inhibiting DNA synthesis, which eventually leads to HeLa cell death.

Sanchez's group reported the Pt-$mSiO_2$ Janus nanomotors as active cargo delivery with different sizes (40, 65, and 90 nm).[43] Fluorescein isothiocyanate (FITC) was used to label the nanomotors by covalent linkages. Small Rhodamine B (RhB) cargo molecules were then loaded into the pores without a Pt-coated side. The confocal laser scanning microscopy (CLSM) observed that the RhB molecules were loaded inside the MNMs (Figure 10b (i)). Using a ratchet shaped microchip comprised of two reservoirs, many drug molecules can be actively transported and delivered to a target chamber in the presence of H_2O_2 fuel compared to passive MSNs (without H_2O_2 fuel). The active diffusion of nanomotors results in enhanced accumulation toward the target reservoir (Figure 10b (ii)).

In addition to the inorganic catalyst Pt-triggered decomposition of H_2O_2, the enzyme is regarded as a more versatile and biocompatible alternative to trigger the biocatalytic decomposition of H_2O_2 and exhibits higher propulsion performance. Máñez and co-workers reported enzyme-powered Au-mesoporous silica Janus-type nanomotors for stimuli-responsive cargo delivery.[111] The Janus nanomotors can be propelled by catalytic decomposition of fuel (H_2O_2) by grafting the catalase enzyme on the Au surface. $Ru(bpy)_3Cl_2$ (bpy = 2,20-bipyridine) cargoes are loaded in the mesopores of silica, and disulfide-linked oligo(ethylene glycol) (SS-OEG) chains as a gatekeeper are coated on the surface, which not only can avoid guest molecules leakage but also offer the gatekeeping of the guest molecules through controlling the opening or closing of the pore entrances. In the presence of glutathione (GSH), the gatekeeper will be open, achieving stimuli-responsive controlled cargo release (Figure 10c (i)). The CLSM observed an enhanced cell internalization, and larger amounts of drugs are released into HeLa cells compared to passive nanoparticles without H_2O_2, which is attributed to self-propulsion and controlled drug release of the gatekeeper (Figure 10c (ii and iii).

3.1.2. Nontoxic Fuel Powered Heterosilica-Based MNMs. Although MNMs driven by the fuel hydrogen peroxide have good movement performance and effective drug delivering capability, H_2O_2 fuel is poisonous to cells.[112] Therefore, a wide range of in vitro and in vivo biomedical applications require more biofriendly fuels to drive the propulsion of the MNMs. Up until now, the source of nontoxic fuels mainly focuses on glucose or urea, which provides a more ideal system for the biocompatibility problem.

Wang and co-workers presented the first example of navigating the enzyme-propelled mesoporous silica nanomotors in oil solution or at the oil−water interface by loading lipase into mesoporous silica nanoparticles. The utilization of lipase not only can power motor motion but also can effectively clear the triglyceride droplets (e.g., tributyrin), offering considerable potential in biomedicine for high triglyceride-related diseases.[113] Patiño demonstrated mesoporous heterosilica-based urease-powered nanomotors with functionalized-anti-$FGFR_3$ on their outer surface.[90] The antibody allows for the specific reorganization and attachment with the bladder cancer cells spheroids (Figure 11a (i)). Immunocytochemistry in Figure 11a (ii) confirms the successful express of targeted antigen ($FGFR_3$) on the surface of the bladder cancer spheroids (green fluorescence represents the transmembrane protein FGFR3 and blue represents the cell nuclei). Fluorescence image of mesoporous silica nano-

https://doi.org/10.1021/acs.chemmater.1c00192
Chem. Mater. 2021, 33, 3022−3046

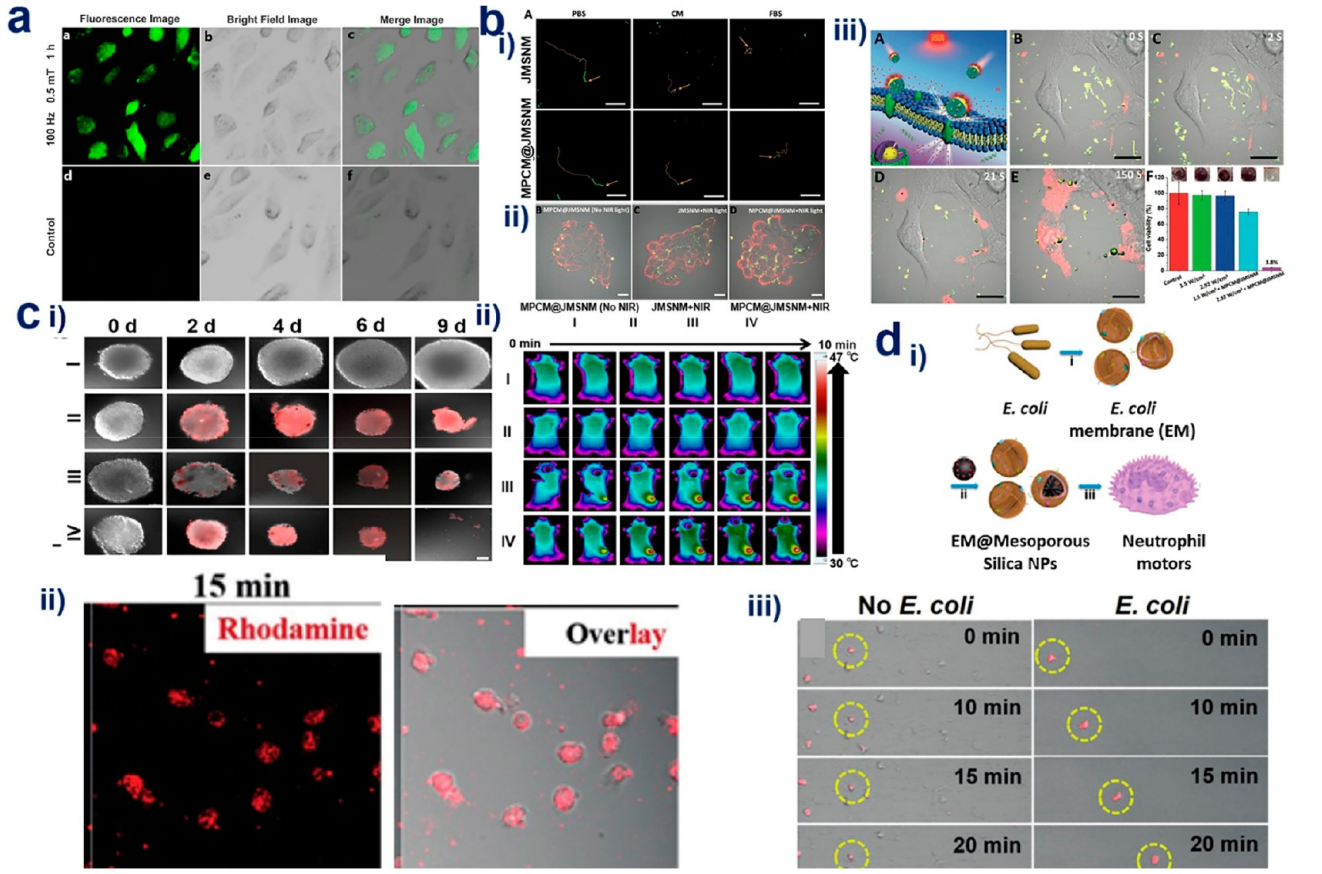

Figure 12. (a) Controlled 6-carboxyfluorescein release of tubelike mesoporous silica nanomotors in HeLa cells. Reprinted with permission from ref 115. Copyright 2015 American Chemical Society. (b) (i) The voyage trajectories of the MPCM-camouflaged nanomotor (bottom) and without bare nanomotor (top) upon NIR light illumination in three different media, scale bars = 20 mm, (ii) enhanced accumulation of MPCM-camouflaged nanomotor on the surface of cancer cells, and (iii) thermomechanical perforation of the cancer cell membranes activated by NIR light. Reprinted with permission from ref 70. Copyright 2018 Wiley-VCH Verlag. (c) (i) Tumor elimination by nanomotors under different treatment conditions for 0−9 days (scale bar = 100 mm) and (ii) in vivo thermal images of tumor-bearing mice at different times under NIR irradiation for 10 min after being injected with different samples. Reprinted with permission from ref 103. Copyright 2020 Wiley-VCH Verlag. (d) (i) Schematic illustration of the preparation of hybrid neutrophil micromotors, (ii) CLSM images of neutrophils incubated with EM@MSNs labeled with Rhodamine 6G for 15 min, scale bars = 20 mm, and (iii) time-lapse CLSM images of hybrid neutrophil micromotors in the presence of *E. coli* (right) and in the absence of *E. coli* (left), scale bars = 50 mm. Reprinted with permission from ref 36. Copyright 2017 Wiley-VCH Verlag.

motor incubated with spheroids at 0 and 40 mM urea showed that active motion improves penetration into the bladder cancer spheroids. Figure 11a (iii) confirmed that antibody-modified nanomotors in the presence of urea show higher internalization efficiency (3-fold higher) than antibody-modified nanomotors in the absence of urea. The combination of active motion ability and the targeted antibody improves the internalization, which is 14 times higher than in the case of passive particles without antibody.

Mesoporous heterosilica-based MNMs have presented enhanced diffusion and high drug loading capacity. However, during the transportation process of cargoes, a non-negligible amount of drug could be leaked before reaching the targeted location, leading to limited drug delivery. Moreover, unspecific cargo release could affect the adjacent normal tissue.

The Sánchez group created molecular gates on the surface of mesoporous silica nanomotors, endowing them with a stimuli-responsive cargo release manner.[114] As shown in Figure 11b (i), MSNs are loaded with different drug molecules, functionalized with benzimidazole groups on the outer surface, and further capped with cyclodextrin-modified urease (CD-U) via the formation of inclusion complexes between CD-U and benzimidazole. Urease triggers the movement of nanomotors in the presence of urea by biocatalytic reaction. Meanwhile, the grafted benzimidazolec:CD-U molecules act as a gatekeeper to achieve "zero" release at physiological pH, whereas delivery is only triggered at acidic pH (4.5−5.5) through the dethreading of the gatekeeper (benzimidazole:CD-U molecules) (Figure 11b (ii)). Figure 11b (iii) shows the delivery of DOX in HeLa cells, and the results indicated that enhanced internalization in the presence of urea due to the active motion of the nanomotors and the ideal drug release inside cells are achieved by a stimuli-responsive gatekeeper.

3.1.3. Fuel-Free MNMs and Biological Cell-Driven MNMs for Drug Delivery. Although significant advances have been made on the propulsion of MNMs using nonbiotoxic or biocompatible, biological cell-driven MNMs or fuel-free MNMs driven by different types of energy sources such as external physical triggers (i.e., light, magnetic, electrical, etc.) are highly expected toward the realistic biomedical applications.

Liu et al. reported on magnetically actuated tubelike mesoporous heterosilica-based MNMs with magnetic $CoFe_2O_4$ nanoparticles.[115] The carboxyfluorescein molecules

https://doi.org/10.1021/acs.chemmater.1c00192
Chem. Mater. 2021, 33, 3022−3046

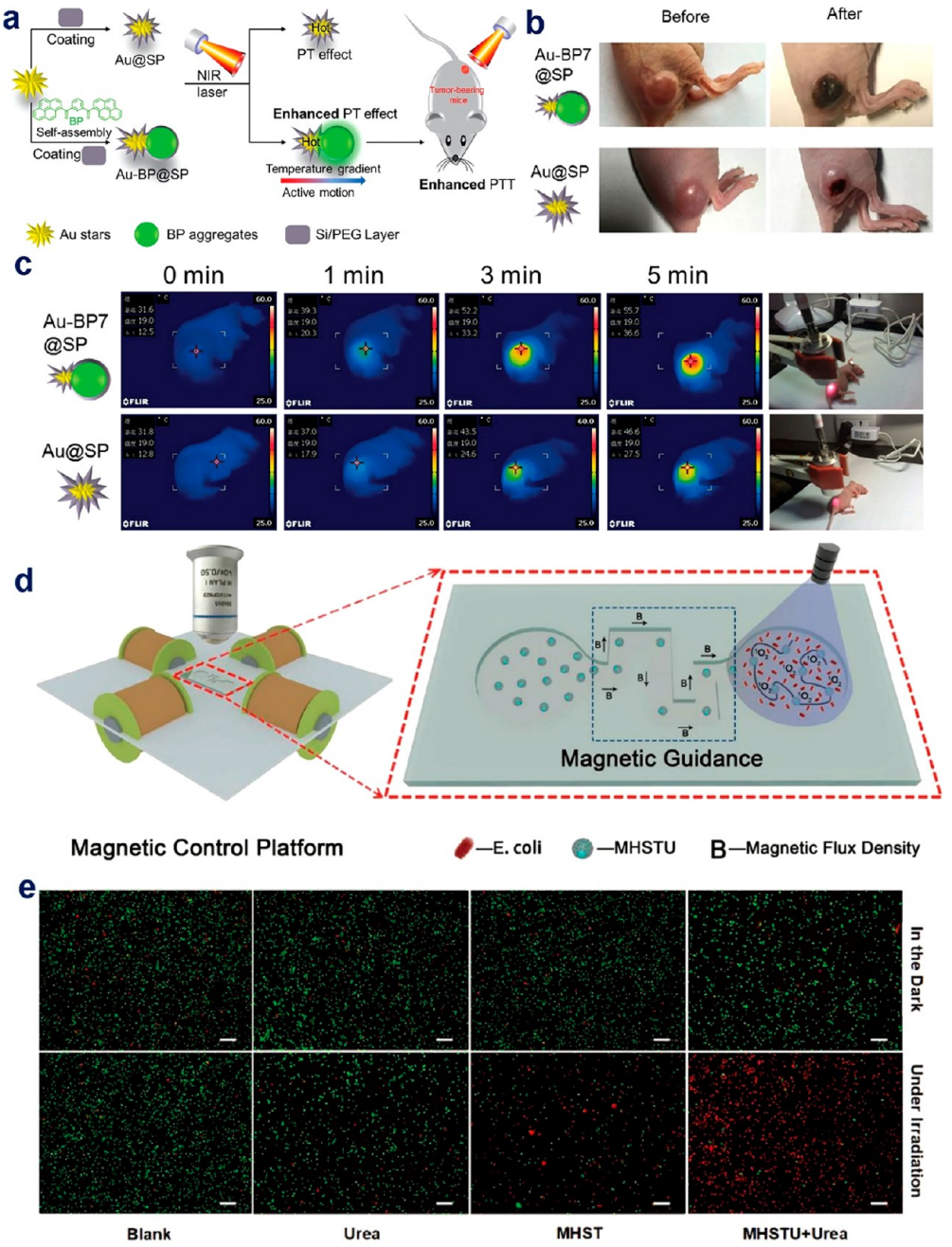

Figure 13. (a) Schematic illustration of a self-propulsion Janus nanomotor for enhanced photothermal tumor therapy under NIR laser irradiation. (b) Representative photos of mice injected Janus nanomotors (top) and Au@SP nanoparticle (bottom). (c) Infrared thermal images of Janus nanomotors and Au@SP nanoparticles injected mice at different time points. Reprinted with permission from ref 118. Copyright 2016 Wiley-VCH Verlag. (d) Control of the movement direction of nanomotors for targeted killing of *E. coli* by a magnetic control platform and (e) fluorescent images showing much higher efficiency of bacteria killing by active carriers. Reprinted with permission from ref 92. Copyright 2019 Wiley-VCH Verlag.

as model payloads were loaded into the nanopores of silica and DNA G-quadruplexes and were further functionalized on the surface of the silica tube to prevent leakage of payloads. The resultant nanomotors with $CoFe_2O_4$ nanoparticles can be heated by an alternating magnetic field, leading to the conformational change of G-quadruplexes and further allowing for the release of carboxyfluorescein into Hela cells (Figure 12a).

Besides magnetic propulsion MNMs, the He group designed a fuel-free near-infrared (NIR) light-powered mesoporous silica/Au Janus nanomotors with a macrophage cell membrane (MPCM) coating.[70] Under NIR light irradiation, a thermal gradient across the Janus motors is generated due to the photothermal effect of the Au shells,[116] generating a self-thermophoretic force to propel the nanomotors (Figure 12b (i)). The two-photon confocal laser scanning microscope (TP-CLSM) images show that MPCM cloaking improves the velocity of the nanomotors in different types of solutions compared to the uncoated Janus nanomotors (without MPCM), suggesting that MPCM cloaking cannot only effectively reduce the adhesion of biomolecules in the media but also improve the target recognition toward cancer cells.

https://doi.org/10.1021/acs.chemmater.1c00192
Chem. Mater. 2021, 33, 3022−3046

Figure 12b (ii) observed that self-propulsion and MPCM coating promote the amount of nanomotors on the surface of cancer cells compared to those cases with no NIR light or MPCM. The green and red fluorescence represents the nanomotors and cancer cell membranes, respectively. They further estimated the generated propulsion force, which is not enough to rupture the cancer cell membrane for drug injection. By increasing the NIR laser intensity, the nanomotors can completely open the pores on the cytomembranes of the cancer cells by the photothermomechanical effect of the nanomotors, leading to irreversible damage of the cytomembrane and the viability decreasing to 3.8% (Figure 12b (iii)). Such multifunctional nanomotors are expected to be used in vivo for effective drug delivery in cancer treatment.

Very recently, another interesting example was proposed by Wei and co-workers.[103] They designed a NIR-driven multidrug loaded silica/Pt nanomotors with hierarchical pores (mesoporous-microporous) for cancer chemo/photothermal therapy. The Pt nanoparticles with 20−40 nm are asymmetrically loaded in microporous silica and generate a thermal gradient due to their unique surface plasmon resonance effect (SPR) under NIR irradiation to propel the nanomotors.[113] Targeted anticancer drug heparin-folate nanoparticles (about 20−40 nm) and DOX are loaded into mesopores and macropores, respectively. In vitro CLSM images and in vivo thermal images confirm that the integration of photothermal effects of Pt, self-propulsion, and targeted drug delivery facilitates tumor elimination (Figure 12c (i and ii). Wan et al. also synthesized similar structured mesoporous/macroporous silica (MMS)/platinum (Pt) nanomotors. They further loaded the thrombolytic drug of urokinase (UK) and an anticoagulant drug of Hep inside the macropores and mesopores of silica, respectively, follow by modification of the platelet membrane (PM). The obtained nanomotors can reach a targeted thrombus site due to the special proteins on PM, and then PM can be ruptured under NIR irradiation to achieve a desirable drug release. Such multifunctional nanomotors with targeting ability and active motion can notably enhance the thrombolysis effect, and the relative thrombus volume can be decreased by the MMNM/Hep/UK/PM.[104]

Alternatively, living organisms with intrinsic chemotactic characteristics have also been employed as the engine to drive biohybrid MNMs. The incorporated biological materials can effectively avoid elimination by the immune system and the biofouling problem.[117] Such self-guided biohybrid MNMs demonstrate great potential for targeted drug transport and delivery without additional fuels. Various therapeutic purposes can be achieved depending on different types of living organisms. The He group proposed biohybrid nanomotors by combining neutrophils with bacteria-membrane-modified mesoporous silica nanospheres, exhibiting a chemotactic motion toward *Escherichia coli* (*E. coli*) (Figure 12 d (i)). *E. coli* membranes camouflaging not only promotes drug encapsulation in mesoporous silica without undesired leakage but also accelerates the endocytosis of neutrophils (Figure 12 d (ii)). The time-lapse CLSM images confirm that biohybrid motors displayed directional movement along the chemoattractant gradients produced by *E. coli* (Figure 12d (iii)).[36] Such biohybrid heterosilica MNMs with good biocompatibility, high drug loading capacity, and chemotactic characteristic could pave the way to new targeted drug delivery.

3.2. Heterosilica-Based MNMs for Cancer Phototherapy (PTT and PDT). Heterosilica-based MNMs can also be used in cancer phototherapy such as PTT and PDT. For example, Wang et al. designed a NIR light propulsive Au-bis-pyrene (BP)@peglated silica (SP) Janus nanomotor.[118] Due to the SPR effect of the Au parts, the obtained nanohybrid shows active motion and enhanced PT effect under NIR light irradiation. The active motion of the nanomotor shows a stronger PT effect than passive nanoparticles by effectively converting the kinetic energy into thermal energy, thereby leading to enhanced cancer cells killing efficiency (Figure 13a). Furthermore, they evaluated the PT effect in vivo, and the representative photos of the mice show that active nanomotors can effectively kill the tumor cells compared to passive nanoparticles (Au@SP) (Figure 13b). The tumor temperature of mice injected with Janus nanomotors (~55.7 °C) is higher than Au@SP nanoparticles (46.6 °C) by infrared thermal images (Figure 13c). These results indicated that the active motion of Janus nanohybrids contributed to PTT of cancer cells. The work opens a new avenue for active photothermal cancer therapy by using self-propelling MNMs.

In addition to PTT, MNMs-based PDT has aroused great attention due to its excellent efficiency. The PDT process mainly relies on reactive oxygen species-mediated cancer cells or bacteria killing produced by light-excited photosensitizer which can activate the surrounding oxygen molecules ($^3O_2$) to generate singlet oxygen ($^1O_2$). Traditional PDT efficiency is often low due to limited availability of $^3O_2$ surrounding the photosensitizer and diffusion range of photoactivated singlet oxygen ($^1O_2$).[119,120] Compared with traditional PDT, self-propelled NMNs can act as a mobile photosensitizer platform, which improves the availability of $^3O_2$ and enlarges diffusion distance of $^1O_2$, giving highly efficient PDT efficacy.

Ma et al. designed an enzyme-powered magnetic hollow mesoporous SiO_2 micromotor with photosensitizer 5,10,15,20-tetrakis(4-aminophenyl)porphyrin (TAPP) loading.[92] In the presence of urea, micromotors are propelled by reactions of enzymes asymmetrically. Furthermore, hollow mesoporous silica motors can achieve remote control on the movement direction under magnetic control platform. Therefore, the loaded TAPP molecules can effectively convert surrounding $^3O_2$ into $^1O_2$ molecules to rapidly spread out, resulting in targeted killing of *E. coli* (Figure 13d). Moreover, the enhanced single oxygen generation capability and enlarged spread area of $^1O_2$ by the active motion of micromotors lead to much higher efficiency of bacteria killing under light irradiation than in the case of passive carriers (green and red fluorescence represent living bacteria and dead bacteria, respectively) (Figure 13e).

■ CONCLUSION

Over the past decade, the development of self-propelled MNMs has presented a variety of opportunities for potential applications in the biomedical field. Silica is the most widely used material in the biomedical field due to its many unique virtues.[121] This review presents a comprehensive and systematic overview of the design of heterosilica-based MNMs and their applications in the biomedical field. A new strategy for the design and construction of heterosilica-based MNMs is also proposed. The core principle is to build asymmetry of geometry, components, or surface properties. These obtained heterosilica-based MNMs possess excellent motion performance and advanced functionality due to their attractive features such as stimuli-responsive behavior, unique pore structure, easy surface functionalization, and ability to be integrated with

https://doi.org/10.1021/acs.chemmater.1c00192
Chem. Mater. 2021, 33, 3022−3046

metal or biocomponents, etc. These beneficial properties make heterosilica-based MNMs powerful and promising micro/nanotools for performing diverse complex biological tasks in future biomedical applications (Figure 14).

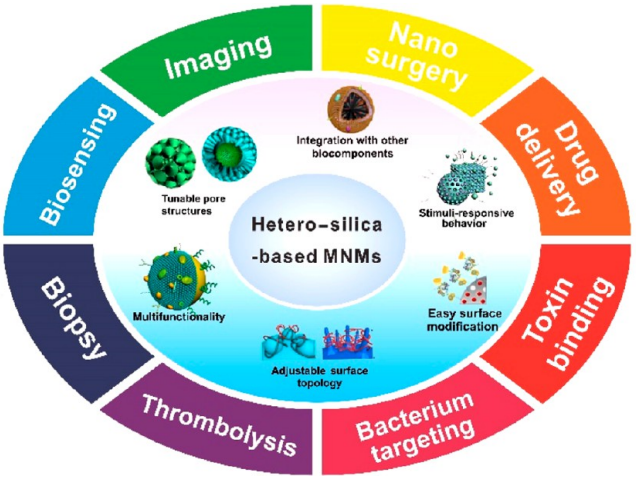

Figure 14. Perspectives of heterosilica-based MNMs for future biomedical applications. Reprinted with permission from refs 25, 36, 70, 114, and 121. Copyright 2014 American Chemical Society, 2017 Wiley-VCH Verlag, 2018 Wiley-VCH Verlag, 2019 American Chemical Society, and 2020 American Chemical Society, respectively.

For real applications of heterosilica-based MNMs in the biomedical field, key challenges still remain unaddressed. Most studies on motion performance have been explored in aqueous solutions. However, they experience relatively large drag force when functioning in a more viscous physiological environment, which could lead to reduced velocity and even undergo mode variation of motion. Existing work has placed a considerable focus on improving motion preformation of heterosilica-based MNMs by controlling the geometry and morphology, but less attention has been paid to their surface properties, we have shown that surface roughness is beneficial for improving the speed. In addition, viruslike heterosilica-based MNMs with spiky surface topology show enhanced cellular uptake efficiency. Therefore, future endeavors should be focused on optimizing surface properties. Developing heterosilica-based MNMs with a higher fuel conversion efficiency is necessary, enabling them to overcome the drag force and reaching target locations. Moreover, cross-disciplinary researches should also be built to better understand the interaction between the active motion and biological media.

Additional effort should also be dedicated to developing smarter and better functionalized heterosilica-based MNMs as ideal drug delivery carriers. For instance, some intelligent ingredients are employed to modify on their surface to perceive changes of the surrounding environment (e.g., temperature, light, magnetic fields, or pH) for autoguidance and stimuli-responsive on-demanding cargo release during treatment. Such capabilities not only could ensure that the heterosilica-based MNMs can effectively reach the targeted diseased sites, minimizing the undesirable side effects on normal cells, but also achieve the safe and efficient transportation of drug cargoes.

Ongoing and future efforts should also focus on biocompatibility issues considering the motors' fates after mission completion and a long-term impact on the body. The biocompatibility of heterosilica-based MNMs primarily relies on the properties of synthetic materials. Silica has been proven to be a biocompatible material. However, its biocompatibility may be reduced when functionalized by foreign organic molecules or inorganic components. Biomimetic heterosilica-based MNMs by functionalizing cellular components have presented a dramatic increase of biocompatibility and biodegradability. In the meanwhile, the incorporated cell materials not only prolong the circulation time of heterosilica-based MNMs in biofluids but also effectively prevent attack from the human system. Additionally, propulsion approaches should be fully biocompatible, which means that they should utilize less toxic or even completely nontoxic fuels, biofriendly external fields, or nonthreatening living organisms (e.g., neutrophils). Also, in vivo tests need to be conducted to evaluate their biosafety ahead of final clinical application.

Taken together, the continuous innovation of fabrication approaches and the promotion of multidisciplinary cooperation provide new opportunities for constructing advanced multifunctional heterosilica-based MNMs. We believe that heterosilica-based MNMs will have a far-reaching impact on the future nanomedicine and biotechnology fields.

AUTHOR INFORMATION

Corresponding Author

Biao Kong − *Department of Chemistry, Shanghai Key Lab of Molecular Catalysis and Innovative Materials, iChEM, Fudan University, Shanghai 200438, P. R. China;* orcid.org/0000-0002-3251-5071; Email: bkong@fudan.edu.cn

Authors

Miao Yan − *Department of Chemistry, Shanghai Key Lab of Molecular Catalysis and Innovative Materials, iChEM, Fudan University, Shanghai 200438, P. R. China;* orcid.org/0000-0002-0546-6630

Lei Xie − *Department of Chemistry, Shanghai Key Lab of Molecular Catalysis and Innovative Materials, iChEM, Fudan University, Shanghai 200438, P. R. China;* orcid.org/0000-0003-4751-4271

Jinyao Tang − *Department of Chemistry, The University of Hong Kong, Hong Kong 999077, China;* orcid.org/0000-0002-0051-148X

Kang Liang − *School of Chemical Engineering, Graduate School of Biomedical Engineering, Australian Centre for NanoMedicine, The University of New South Wales, Sydney, New South Wales 2052, Australia;* orcid.org/0000-0003-3985-7688

Yongfeng Mei − *Department of Materials Science and State Key Laboratory of ASIC and System, Fudan University, Shanghai 200433, China;* orcid.org/0000-0002-3314-6108

Complete contact information is available at: https://pubs.acs.org/10.1021/acs.chemmater.1c00192

Author Contributions

All authors have given approval to the final version of the manuscript.

Notes

The authors declare no competing financial interest.

https://doi.org/10.1021/acs.chemmater.1c00192
Chem. Mater. 2021, 33, 3022−3046

■ ACKNOWLEDGMENTS

This work was supported by the National Key Research and Development Program of China (2019YFC1604601, 2019YFC1604600, 2017YFA0206901, 2017YFA0206900, and 2018YFC1602301), the National Natural Science Foundation of China (21705027, 21974029, and 51961145108), the Natural Science Foundation of Shanghai (18ZR1404700), and Construction project of Shanghai Key Laboratory of Molecular Imaging(18DZ2260400), Shanghai Municipal Education Commission (Class II Plateau Disciplinary Construction Program of Medical Technology of SUMHS, 2018-2020).

■ REFERENCES

(1) Hess, H. Engineering applications of biomolecular motors. *Annu. Rev. Biomed. Eng.* **2011**, *13*, 429−450.
(2) Hess, H.; Saper, G. Engineering with biomolecular motors. *Acc. Chem. Res.* **2018**, *51*, 3015−3022.
(3) Furuta, A.; Amino, M.; Yoshio, M.; Oiwa, K.; Kojima, H.; Furuta, K. Creating biomolecular motors based on dynein and actin-binding proteins. *Nat. Nanotechnol.* **2017**, *12*, 233−237.
(4) Yu, G.; Yung, B. C.; Zhou, Z.; Mao, Z.; Chen, X. Artificial mo lecular machines in nanotheranostics. *ACS Nano* **2018**, *12*, 7−12.
(5) Browne, W. R.; Feringa, B. L. Making molecular machines work. *Nat. Nanotechnol.* **2006**, *1*, 25−35.
(6) Richards, V. 2016 Nobel Prize in chemistry: molecular machines. *Nat. Chem.* **2016**, *8*, 1090.
(7) Jiang, S.; Kaltbeitzel, A.; Hu, M.; Suraeva, O.; Crespy, D.; Landfester, K. One-step preparation of fuel-containing anisotropic nanocapsules with stimuli-regulated propulsion. *ACS Nano* **2020**, *14*, 498−508.
(8) Ou, J.; Liu, K.; Jiang, J.; Wilson, D. A.; Liu, L.; Wang, F.; Wang, S.; Tu, Y.; Peng, F. Micro-/nanomotors toward biomedical applications: the recent progress in biocompatibility. *Small* **2020**, *16*, 1906184.
(9) Peng, F.; Tu, Y.; van Hest, J. C.; Wilson, D. A. Self-guided supramolecular cargo-loaded nanomotors with chemotactic behavior towards cells. *Angew. Chem., Int. Ed.* **2015**, *54*, 11662−11665.
(10) Abdelmohsen, L. K.; Nijemeisland, M.; Pawar, G. M.; Janssen, G. J.; Nolte, R. J.; van Hest, J. C.; Wilson, D. A. Dynamic loading and unloading of proteins in polymeric stomatocytes: formation of an enzyme-loaded supramolecular nanomotor. *ACS Nano* **2016**, *10*, 2652−2660.
(11) Liang, C.; Zhan, C.; Zeng, F.; Xu, D.; Wang, Y.; Zhao, W.; Zhang, J.; Guo, J.; Feng, H.; Ma, X. Bilayer tubular micromotors for simultaneous environmental monitoring and remediation. *ACS Appl. Mater. Interfaces* **2018**, *10*, 35099−35107.
(12) Giudicatti, S.; Marz, S. M.; Soler, L.; Madani, A.; Jorgensen, M. R.; Sanchez, S.; Schmidt, O. G. Photoactive rolled-up TiO_2 microtubes: fabrication, characterization and applications. *J. Mater. Chem. C* **2014**, *2*, 5892−5901.
(13) Wang, Y.; Zhou, C.; Wang, W.; Xu, D.; Zeng, F.; Zhan, C.; Gu, J.; Li, M.; Zhao, W.; Zhang, J.; Guo, J.; Feng, H.; Ma, X. Photocatalytically powered matchlike nanomotor for light-guided active SERS sensing. *Angew. Chem., Int. Ed.* **2018**, *57*, 13110−13113.
(14) Chen, C.; Chang, X.; Teymourian, H.; Ramirez-Herrera, D. E.; Esteban-Fernandez de Avila, B.; Lu, X.; Li, J.; He, S.; Fang, C.; Liang, Y.; Mou, F.; Guan, J.; Wang, J. Bioinspired chemical communication between synthetic nanomotors. *Angew. Chem., Int. Ed.* **2018**, *57*, 241−245.
(15) Ren, L.; Nama, N.; McNeill, J. M.; Soto, F.; Yan, Z.; Liu, W.; Wang, W.; Wang, J.; Mallouk, T. E. 3D steerable, acoustically powered microswimmers for single-particle manipulation. *Sci. Adv.* **2019**, *5*, eaax3084.
(16) Soto, F.; Wang, J.; Ahmed, R.; Demirci, U. Medical micro/nanorobots in precision medicine. *Adv. Sci.* **2020**, *7*, 2002203.
(17) Wu, Z.; Chen, Y.; Mukasa, D.; Pak, O. S.; Gao, W. Medical micro/nanorobots in complex media. *Chem. Soc. Rev.* **2020**, *49*, 8088.
(18) Peng, F.; Tu, Y.; Wilson, D. A. Micro/nanomotors towards in vivo application: cell, tissue and biofluid. *Chem. Soc. Rev.* **2017**, *46*, 5289−5310.
(19) Li, J.; Esteban-Fernández de Ávila, B.; Gao, W.; Zhang, L.; Wang, J. Micro/nanorobots for biomedicine: Delivery, surgery, sensing, and detoxification. *Sci. Robot.* **2017**, *2*, eaam6431.
(20) Reinisova, L.; Hermanova, S.; Pumera, M. Micro/nanomachines: what is needed for them to become a real force in cancer therapy? *Nanoscale* **2019**, *11*, 6519−6532.
(21) Yang, Y.; Zhang, M.; Song, H.; Yu, C. Silica-based nanoparticles for biomedical applications: from nanocarriers to biomodulators. *Acc. Chem. Res.* **2020**, *53*, 1545−1556.
(22) Sun, B.; Wang, X.; Liao, Y. P.; Ji, Z.; Chang, C. H.; Pokhrel, S.; Ku, J.; Liu, X.; Wang, M.; Dunphy, D. R.; Li, R.; Meng, H.; Madler, L.; Brinker, C. J.; Nel, A. E.; Xia, T. Repetitive dosing of fumed silica leads to profibrogenic effects through unique structure-activity relationships and biopersistence in the lung. *ACS Nano* **2016**, *10*, 8054−8066.
(23) Gao, M.; Zeng, J.; Liang, K.; Zhao, D.; Kong, B. Interfacial assembly of mesoporous silica-based optical heterostructures for sensing applications. *Adv. Funct. Mater.* **2020**, *30*, 1906950.
(24) Kankala, R. K.; Han, Y.-H.; Na, J.; Lee, C.-H.; Sun, Z.; Wang, S.-B.; Kimura, T.; Ok, Y. S.; Yamauchi, Y.; Chen, A.-Z.; Wu, K. C. W. Nanoarchitectured structure and surface biofunctionality of mesoporous silica nanoparticles. *Adv. Mater.* **2020**, *32*, 1907035.
(25) Zhao, T.; Elzatahry, A.; Li, X.; Zhao, D. Single-micelle-directed synthesis of mesoporous materials. *Nat. Rev. Mater.* **2019**, *4*, 775−791.
(26) Ahmad Nor, Y.; Niu, Y.; Karmakar, S.; Zhou, L.; Xu, C.; Zhang, J.; Zhang, H.; Yu, M.; Mahony, D.; Mitter, N.; Cooper, M. A.; Yu, C. Shaping nanoparticles with hydrophilic compositions and hydrophobic properties as nanocarriers for antibiotic delivery. *ACS Cent. Sci.* **2015**, *1*, 328−334.
(27) Niu, Y.; Yu, M.; Hartono, S. B.; Yang, J.; Xu, H.; Zhang, H.; Zhang, J.; Zou, J.; Dexter, A.; Gu, W.; Yu, C. Nanoparticles mimicking viral surface topography for enhanced cellular delivery. *Adv. Mater.* **2013**, *25*, 6233−6237.
(28) Zhang, B.; Huang, G.; Wang, L.; Wang, T.; Liu, L.; Di, Z.; Liu, X.; Mei, Y. Rolled-up monolayer graphene tubular micromotors: enhanced performance and antibacterial property. *Chem. - Asian J.* **2019**, *14*, 2479−2484.
(29) Zhang, X.; Chen, C.; Wu, J.; Ju, H. Bubble-propelled jellyfish-like micromotors for DNA sensing. *ACS Appl. Mater. Interfaces* **2019**, *11*, 13581−13588.
(30) Zhang, H.; Duan, W.; Liu, L.; Sen, A. Depolymerization-powered autonomous motors using biocompatible fuel. *J. Am. Chem. Soc.* **2013**, *135*, 15734−15737.
(31) Qin, W.; Peng, T.; Gao, Y.; Wang, F.; Hu, X.; Wang, K.; Shi, J.; Li, D.; Ren, J.; Fan, C. Catalysis-driven self-thermophoresis of Janus plasmonic nanomotors. *Angew. Chem., Int. Ed.* **2017**, *56*, 515−518.
(32) Xuan, M.; Wu, Z.; Shao, J.; Dai, L.; Si, T.; He, Q. Near infrared light-powered Janus mesoporous silica nanoparticle motors. *J. Am. Chem. Soc.* **2016**, *138*, 6492−6497.
(33) Wang, J.; Xiong, Z.; Zhan, X.; Dai, B.; Zheng, J.; Liu, J.; Tang, J. A silicon nanowire as a spectrally tunable light-driven nanomotor. *Adv. Mater.* **2017**, *29*, 1701451.
(34) Velegol, D.; Garg, A.; Guha, R.; Kar, A.; Kumar, M. Origins of concentration gradients for diffusiophoresis. *Soft Matter* **2016**, *12*, 4686−4703.
(35) Hu, C. M.; Fang, R. H.; Copp, J.; Luk, B. T.; Zhang, L. A biomimetic nanosponge that absorbs pore-forming toxins. *Nat. Nanotechnol.* **2013**, *8*, 336−340.
(36) Shao, J.; Xuan, M.; Zhang, H.; Lin, X.; Wu, Z.; He, Q. Chemotaxis-guided hybrid neutrophil micromotors for targeted drug transport. *Angew. Chem., Int. Ed.* **2017**, *56*, 12935−12939.
(37) Schmidt, C. K.; Medina-Sanchez, M.; Edmondson, R. J.; Schmidt, O. G. Engineering microrobots for targeted cancer therapies from a medical perspective. *Nat. Commun.* **2020**, *11*, 5618.

https://doi.org/10.1021/acs.chemmater.1c00192
Chem. Mater. 2021, 33, 3022−3046

(38) Gao, W.; Wang, J. Synthetic micro/nanomotors in drug delivery. *Nanoscale* **2014**, *6*, 10486−10494.
(39) Wang, S.; Liu, K.; Wang, F.; Peng, F.; Tu, Y. The Application of micro- and nanomotors in classified drug delivery. *Chem. - Asian J.* **2019**, *14*, 2336−2347.
(40) Xu, D.; Wang, Y.; Liang, C.; You, Y.; Sanchez, S.; Ma, X. Self-propelled micro/nanomotors for on-demand biomedical cargo transportation. *Small* **2020**, *16*, 1902464.
(41) Wan, M.; Li, T.; Chen, H.; Mao, C.; Shen, J. Biosafety, functionalities and applications of biomedical micro/nanomotors. *Angew. Chem., Int. Ed. Engl.* **2020**, DOI: 10.1002/anie.202013689.
(42) Lin, X.; Xu, B.; Zhu, H.; Liu, J.; Solovev, A.; Mei, Y. Requirement and development of hydrogel micromotors towards biomedical applications. *Research (Wash. D. C.)* **2020**, *2020*, 7659749.
(43) Ma, X.; Hahn, K.; Sanchez, S. Catalytic mesoporous Janus nanomotors for active cargo delivery. *J. Am. Chem. Soc.* **2015**, *137*, 4976−4979.
(44) Lee, T. C.; Alarcon-Correa, M.; Miksch, C.; Hahn, K.; Gibbs, J. G.; Fischer, P. Self-propelling nanomotors in the presence of strong Brownian forces. *Nano Lett.* **2014**, *14*, 2407−2412.
(45) Pourrahimi, A. M.; Pumera, M. Multifunctional and self-propelled spherical Janus nano/micromotors: recent advances. *Nanoscale* **2018**, *10*, 16398−16415.
(46) Vu, T. D.; Chen, Z.; Zeng, X.; Jiang, M.; Liu, S.; Gao, Y.; Long, Y. Physical vapour deposition of vanadium dioxide for thermochromic smart window applications. *J. Mater. Chem. C* **2019**, *7*, 2121−2145.
(47) Xu, L.; Mou, F.; Gong, H.; Luo, M.; Guan, J. Light-driven micro/nanomotors: from fundamentals to applications. *Chem. Soc. Rev.* **2017**, *46*, 6905−6926.
(48) Archer, R. J.; Parnell, A. J.; Campbell, A. I.; Howse, J. R.; Ebbens, S. J. A Pickering Emulsion Route to Swimming Active Janus Colloids. *Adv. Sci.* **2018**, *5*, 1700528.
(49) Lv, H.; Xing, Y.; Du, X.; Xu, T.; Zhang, X. Construction of dendritic Janus nanomotors with H_2O_2 and NIR light dual-propulsion via Pickering emulsion. *Soft Matter* **2020**, *16*, 4961−4968.
(50) Gao, S.; Hou, J. w.; Zeng, J.; Richardson, J. J.; Gu, Z.; Gao, X.; Li, D. W.; Gao, M.; Wang, D. W.; Chen, P.; Chen, V.; Liang, K.; Zhao, D.; Kong, B. Superassembled biocatalytic porous framework micromotors with reversible and sensitive pH-speed regulation at ultralow physiological H_2O_2 concentration. *Adv. Funct. Mater.* **2019**, *29*, 1808900.
(51) Gibbs, J. G.; Zhao, Y. P. Autonomously motile catalytic nanomotors by bubble propulsion. *Appl. Phys. Lett.* **2009**, *94*, 163104.
(52) Schattling, P. S.; Ramos-Docampo, M. A.; Salgueirino, V.; Stadler, B. Double-fueled Janus swimmers with magnetotactic behavior. *ACS Nano* **2017**, *11*, 3973−3983.
(53) Patino, T.; Feiner-Gracia, N.; Arque, X.; Miguel-Lopez, A.; Jannasch, A.; Stumpp, T.; Schaffer, E.; Albertazzi, L.; Sanchez, S. Influence of enzyme quantity and distribution on the self-propulsion of non-Janus urease-powered micromotors. *J. Am. Chem. Soc.* **2018**, *140*, 7896−7903.
(54) Baraban, L.; Makarov, D.; Streubel, R.; Mönch, I.; Grimm, D.; Sanchez, S.; Schmidt, O. G. Catalytic Janus motors on microfluidic chip: deterministic motion for targeted cargo delivery. *ACS Nano* **2012**, *6*, 3383−3389.
(55) Valadares, L. F.; Tao, Y. G.; Zacharia, N. S.; Kitaev, V.; Galembeck, F.; Kapral, R.; Ozin, G. A. Catalytic nanomotors: self-propelled sphere dimers. *Small* **2010**, *6*, 565−572.
(56) Wang, Y.; Fei, S. T.; Byun, Y. M.; Lammert, P. E.; Crespi, V. H.; Sen, A.; Mallouk, T. E. Dynamic interactions between fast microscale rotors. *J. Am. Chem. Soc.* **2009**, *131*, 9926−9927.
(57) Schamel, D.; Pfeifer, M.; Gibbs, J. G.; Miksch, B.; Mark, A. G.; Fischer, P. Chiral colloidal molecules and observation of the propeller effect. *J. Am. Chem. Soc.* **2013**, *135*, 12353−12359.
(58) Gibbs, J. G.; Zhao, Y. P. Design and characterization of rotational multicomponent catalytic nanomotors. *Small* **2009**, *5*, 2304−2308.
(59) Gibbs, J. G.; Zhao, Y. Self-organized multiconstituent catalytic nanomotors. *Small* **2010**, *6*, 1656−1662.
(60) Gibbs, J. G.; Fischer, P. Active colloidal microdrills. *Chem. Commun.* **2015**, *51*, 4192−4195.
(61) Gibbs, J. G.; Fragnito, N. A.; Zhao, Y. Asymmetric Pt/Au coated catalytic micromotors fabricated by dynamic shadowing growth. *Appl. Phys. Lett.* **2010**, *97*, 253107.
(62) Argyo, C.; Weiss, V.; Bräuchle, C.; Bein, T. Multifunctional mesoporous silica nanoparticles as a universal platform for drug delivery. *Chem. Mater.* **2014**, *26*, 435−451.
(63) Tong, F.; Ye, Y.; Chen, B.; Gao, J.; Liu, L.; Ou, J.; van Hest, J. C. M.; Liu, S.; Peng, F.; Tu, Y. Bone-targeting prodrug mesoporous silica-based nanoreactor with reactive oxygen species burst for enhanced chemotherapy. *ACS Appl. Mater. Interfaces* **2020**, *12*, 34630−34642.
(64) Huang, C. C.; Huang, W.; Yeh, C. S. Shell-by-shell synthesis of multi-shelled mesoporous silica nanospheres for optical imaging and drug delivery. *Biomaterials* **2011**, *32*, 556−564.
(65) Li, X.; Zhou, L.; Wei, Y.; El-Toni, A. M.; Zhang, F.; Zhao, D. Anisotropic growth-induced synthesis of dual-compartment Janus mesoporous silica nanoparticles for bimodal triggered drugs delivery. *J. Am. Chem. Soc.* **2014**, *136*, 15086−15092.
(66) Dai, L.; Zhang, Q.; Li, J.; Shen, X.; Mu, C.; Cai, K. Dendrimerlike mesoporous silica nanoparticles as pH-responsive nanocontainers for targeted drug delivery and bioimaging. *ACS Appl. Mater. Interfaces* **2015**, *7*, 7357−7372.
(67) Ma, X.; Feng, H.; Liang, C.; Liu, X.; Zeng, F.; Wang, Y. Mesoporous silica as micro/nano-carrier: from passive to active cargo delivery, a mini review. *J. Mater. Sci. Technol.* **2017**, *33*, 1067−1074.
(68) Hu, S.; Shao, S.; Chen, H.; Sun, J.; Zhai, J.; Zheng, H.; Wan, M.; Liu, Y.; Mao, C.; Zhao, J. Preparation and properties of Janus heparin-loaded ammoniated-hollow mesoporous silica nanomotors. *J. Phys. Chem. C* **2018**, *122*, 9680−9687.
(69) Gao, W.; Pei, A.; Dong, R.; Wang, J. Catalytic iridium-based Janus micromotors powered by ultralow levels of chemical fuels. *J. Am. Chem. Soc.* **2014**, *136*, 2276−2279.
(70) Xuan, M.; Shao, J.; Gao, C.; Wang, W.; Dai, L.; He, Q. Self-Propelled Nanomotors for Thermomechanically percolating cell membranes. *Angew. Chem., Int. Ed.* **2018**, *57*, 12463−12467.
(71) Xuan, M.; Shao, J.; Lin, X.; Dai, L.; He, Q. Self-propelled Janus mesoporous silica nanomotors with sub-100 nm diameters for drug encapsulation and delivery. *ChemPhysChem* **2014**, *15*, 2255−2260.
(72) Ma, X.; Jang, S.; Popescu, M. N.; Uspal, W. E.; Miguel-Lopez, A.; Hahn, K.; Kim, D. P.; Sanchez, S. Reversed Janus micro/nanomotors with internal chemical engine. *ACS Nano* **2016**, *10*, 8751−8759.
(73) Ma, X.; Sanchez, S. A bio-catalytically driven Janus mesoporous silica cluster motor with magnetic guidance. *Chem. Commun.* **2015**, *51*, 5467−5470.
(74) Choudhury, U.; Soler, L.; Gibbs, J. G.; Sanchez, S.; Fischer, P. Surface roughness-induced speed increase for active Janus micromotors. *Chem. Commun.* **2015**, *51*, 8660−8663.
(75) Ma, X.; Sánchez, S. Bio-catalytic mesoporous Janus nanomotors powered by catalase enzyme. *Tetrahedron* **2017**, *73*, 4883−4886.
(76) Wang, Z.; Akter Monny, S.; Wang, L. Hollow structure for photocatalytic CO_2 reduction. *ChemNanoMat* **2020**, *6*, 881−888.
(77) Strandwitz, N. C.; Stucky, G. D. Hollow microporous cerium oxide spheres templated by colloidal silica. *Chem. Mater.* **2009**, *21*, 4577−4582.
(78) Chen, J. S.; Luan, D.; Li, C. M.; Boey, F. Y.; Qiao, S.; Lou, X. W. TiO_2 and SnO_2@TiO_2 hollow spheres assembled from anatase TiO_2 nanosheets with enhanced lithium storage properties. *Chem. Commun.* **2009**, *46*, 8252−8254.
(79) Dergunov, S. A.; Durbin, J.; Pattanaik, S.; Pinkhassik, E. pH-mediated catch and release of charged molecules with porous hollow nanocapsules. *J. Am. Chem. Soc.* **2014**, *136*, 2212−2215.
(80) Han, F.; Wang, R.; Feng, Y.; Wang, S.; Liu, L.; Li, X.; Han, Y.; Chen, H. On demand synthesis of hollow fullerene nanostructures. *Nat. Commun.* **2019**, *10*, 1548.

(81) Lian, M.; Xue, Z.; Qiao, X.; Liu, C.; Zhang, S.; Li, X.; Huang, C.; Song, Q.; Yang, W.; Chen, X.; Wang, T. Movable hollow nanoparticles as reactive oxygen scavengers. *Chem.* **2019**, *5*, 2378−2387.
(82) Li, X.; Zhou, L.; Wei, Y.; El-Toni, A. M.; Zhang, F.; Zhao, D. Anisotropic encapsulation-induced synthesis of asymmetric single-hole mesoporous nanocages. *J. Am. Chem. Soc.* **2015**, *137*, 5903−5906.
(83) Mei, Y.; Solovev, A. A.; Sanchez, S.; Schmidt, O. G. Rolled-up nanotech on polymers: from basic perception to self-propelled catalytic microengines. *Chem. Soc. Rev.* **2011**, *40*, 2109−2119.
(84) Wu, Y.; Lin, X.; Wu, Z.; Mohwald, H.; He, Q. Self-propelled polymer multilayer Janus capsules for effective drug delivery and light-triggered release. *ACS Appl. Mater. Interfaces* **2014**, *6*, 10476−10481.
(85) Li, C.; Zhang, J.; Wang, S.; Zhu, Z.; Li, H.; Xu, A.-B.; Yu, Y.; Wang, X.; Yao, J.; Wang, L.; Solovev, A. A.; He, L. Silica nanocapsules with unusual shapes accessed by simultaneous growth of the template and silica nanostructure. *Chem. Mater.* **2020**, *32*, 575−581.
(86) Ma, X.; Jannasch, A.; Albrecht, U. R.; Hahn, K.; Miguel-Lopez, A.; Schaffer, E.; Sanchez, S. Enzyme-powered hollow mesoporous Janus nanomotors. *Nano Lett.* **2015**, *15*, 7043−50.
(87) Ma, X.; Wang, X.; Hahn, K.; Sanchez, S. Motion control of urea-powered biocompatible hollow microcapsules. *ACS Nano* **2016**, *10*, 3597−3605.
(88) Arque, X.; Romero-Rivera, A.; Feixas, F.; Patino, T.; Osuna, S.; Sanchez, S. Intrinsic enzymatic properties modulate the self-propulsion of micromotors. *Nat. Commun.* **2019**, *10*, 2826.
(89) Wang, H.; Pumera, M. Micro/nanomachines and living biosystems: from simple interactions to microcyborgs. *Adv. Funct. Mater.* **2018**, *28*, 1705421.
(90) Hortelao, A. C.; Carrascosa, R.; Murillo-Cremaes, N.; Patino, T.; Sanchez, S. Targeting 3D bladder cancer spheroids with urease-powered nanomotors. *ACS Nano* **2019**, *13*, 429−439.
(91) Patino, T.; Porchetta, A.; Jannasch, A.; Llado, A.; Stumpp, T.; Schaffer, E.; Ricci, F.; Sanchez, S. Self-sensing enzyme-powered micromotors equipped with pH-responsive DNA nanoswitches. *Nano Lett.* **2019**, *19*, 3440−3447.
(92) Xu, D.; Zhou, C.; Zhan, C.; Wang, Y.; You, Y.; Pan, X.; Jiao, J.; Zhang, R.; Dong, Z.; Wang, W.; Ma, X. Enzymatic micromotors as a mobile photosensitizer platform for highly efficient on-chip targeted antibacteria photodynamic therapy. *Adv. Funct. Mater.* **2019**, *29*, 1807727.
(93) Wang, Q.; Wang, Y.; Guo, B.; Shao, S.; Yu, Y.; Zhu, X.; Wan, M.; Zhao, B.; Bo, C.; Mao, C. Novel heparin-loaded mesoporous tubular micromotors formed via template-assisted electrochemical deposition. *J. Mater. Chem. B* **2019**, *7*, 2688−2695.
(94) Ma, X.; Hortelao, A. C.; Miguel-Lopez, A.; Sanchez, S. Bubble-free propulsion of ultrasmall tubular nanojets powered by biocatalytic reactions. *J. Am. Chem. Soc.* **2016**, *138*, 13782−13785.
(95) Rao, Q.; Si, T.; Wu, Z.; Xuan, M.; He, Q. A Light-activated explosive micropropeller. *Sci. Rep.* **2017**, *7*, 4621.
(96) Yi, D.; Zhang, Q.; Liu, Y.; Song, J.; Tang, Y.; Caruso, F.; Wang, Y. Synthesis of chemically asymmetric silica nanobottles and their application for cargo loading and as nanoreactors and nanomotors. *Angew. Chem., Int. Ed.* **2016**, *55*, 14733−14737.
(97) Li, L.; Wang, J.; Li, T.; Song, W.; Zhang, G. A unified model of drag force for bubble-propelled catalytic micro/nano-motors with different geometries in low Reynolds number flows. *J. Appl. Phys.* **2015**, *117*, 104308.
(98) Liu, Y.; Goebl, J.; Yin, Y. Templated synthesis of nano-structured materials. *Chem. Soc. Rev.* **2013**, *42*, 2610−2653.
(99) Gao, Y.; Dullens, R. P. A.; Aarts, D. Bulk synthesis of silver-head colloidal rodlike micromotors. *Soft Matter* **2018**, *14*, 7119−7125.
(100) Kim, J. H.; Hwang, H. J.; Oh, J. S.; Sacanna, S.; Yi, G. R. Monodisperse magnetic silica hexapods. *J. Am. Chem. Soc.* **2018**, *140*, 9230−9235.
(101) Morgan, A. R.; Dawson, A. B.; McKenzie, H. S.; Skelhon, T. S.; Beanland, R.; Franks, H. P. W.; Bon, S. A. F. Chemotaxis of catalytic silica-manganese oxide "matchstick" particles. *Mater. Horiz.* **2014**, *1*, 65−68.
(102) Abbaraju, P. L.; Meka, A. K.; Song, H.; Yang, Y.; Jambhrunkar, M.; Zhang, J.; Xu, C.; Yu, M.; Yu, C. Asymmetric silica nanoparticles with tunable head-tail structures enhance hemocompatibility and maturation of immune cells. *J. Am. Chem. Soc.* **2017**, *139*, 6321−6328.
(103) Wan, M.; Wang, Q.; Li, X.; Xu, B.; Fang, D.; Li, T.; Yu, Y.; Fang, L.; Wang, Y.; Wang, M.; Wang, F.; Mao, C.; Shen, J.; Wei, J. Systematic research and evaluation models of nanomotors for cancer combined therapy. *Angew. Chem., Int. Ed.* **2020**, *59*, 14458−14465.
(104) Wan, M.; Wang, Q.; Wang, R.; Wu, R.; Li, T.; Fang, D.; Huang, Y.; Yu, Y.; Fang, L.; Wang, X.; Zhang, Y.; Miao, Z.; Zhao, B.; Wang, F.; Mao, C.; Jiang, Q.; Xu, X.; Shi, D. Platelet-derived porous nanomotor for thrombus therapy. *Sci. Adv.* **2020**, *6*, eaaz9014.
(105) Wang, Y.; He, J.; Liu, C.; Chong, W. H.; Chen, H. Thermody namics versus kinetics in nanosynthesis. *Angew. Chem., Int. Ed.* **2015**, *54*, 2022−2051.
(106) Feng, Y.; He, J.; Wang, H.; Tay, Y. Y.; Sun, H.; Zhu, L.; Chen, H. An unconventional role of ligand in continuously tuning of metal-metal interfacial strain. *J. Am. Chem. Soc.* **2012**, *134*, 2004−2007.
(107) Wang, W.; Wang, P.; Chen, L.; Zhao, M.; Hung, C.-T.; Yu, C.; Al-Khalaf, A. A.; Hozzein, W. N.; Zhang, F.; Li, X.; Zhao, D. Engine-trailer-structured nanotrucks for efficient nano-bio interactions and bioimaging-guided drug delivery. *Chem.* **2020**, *6*, 1097−1112.
(108) Zhang, L.; Zhang, F.; Dong, W. F.; Song, J. F.; Huo, Q. S.; Sun, H. B. Magnetic-mesoporous Janus nanoparticles. *Chem. Commun.* **2011**, *47*, 1225−1227.
(109) Poon, W.; Kingston, B. R.; Ouyang, B.; Ngo, W.; Chan, W. C. W. A framework for designing delivery systems. *Nat. Nanotechnol.* **2020**, *15*, 819−829.
(110) Lin, X.; Wu, Z.; Wu, Y.; Xuan, M.; He, Q. Self-propelled micro-/nanomotors based on controlled assembled architectures. *Adv. Mater.* **2016**, *28*, 1060−1072.
(111) Llopis-Lorente, A.; Garcia-Fernandez, A.; Lucena-Sanchez, E.; Diez, P.; Sancenon, F.; Villalonga, R.; Wilson, D. A.; Martinez-Manez, R. Stimulus-responsive nanomotors based on gated enzyme-powered Janus Au-mesoporous silica nanoparticles for enhanced cargo delivery. *Chem. Commun.* **2019**, *55*, 13164−13167.
(112) Wang, S.; Liu, X.; Wang, Y.; Xu, D.; Liang, C.; Guo, J.; Ma, X. Biocompatibility of artificial micro/nanomotors for use in biomedicine. *Nanoscale* **2019**, *11*, 14099−14112.
(113) Wang, L.; Hortelão, A. C.; Huang, X.; Sánchez, S. Lipase-powered mesoporous silica nanomotors for triglyceride degradation. *Angew. Chem., Int. Ed.* **2019**, *58*, 7992−7996.
(114) Llopis-Lorente, A.; Garcia-Fernandez, A.; Murillo-Cremaes, N.; Hortelao, A. C.; Patino, T.; Villalonga, R.; Sancenon, F.; Martinez-Manez, R.; Sanchez, S. Enzyme-powered gated mesoporous silica nanomotors for on-command intracellular payload delivery. *ACS Nano* **2019**, *13*, 12171−12183.
(115) Liu, M.; Pan, L.; Piao, H.; Sun, H.; Huang, X.; Peng, C.; Liu, Y. Magnetically actuated wormlike nanomotors for controlled cargo release. *ACS Appl. Mater. Interfaces* **2015**, *7*, 26017−26021.
(116) Espinosa, A.; Curcio, A.; Cabana, S.; Radtke, G.; Bugnet, M.; Kolosnjaj-Tabi, J.; Pechoux, C.; Alvarez-Lorenzo, C.; Botton, G. A.; Silva, A. K. A.; Abou-Hassan, A.; Wilhelm, C. Intracellular biodegradation of Ag nanoparticles, storage in ferritin, and protection by a Au shell for enhanced photothermal therapy. *ACS Nano* **2018**, *12*, 6523−6535.
(117) Sun, L.; Yu, Y.; Chen, Z.; Bian, F.; Ye, F.; Sun, L.; Zhao, Y. Biohybrid robotics with living cell actuation. *Chem. Soc. Rev.* **2020**, *49*, 4043−4069.
(118) Yang, P. P.; Zhai, Y. G.; Qi, G. B.; Lin, Y. X.; Luo, Q.; Yang, Y.; Xu, A. P.; Yang, C.; Li, Y. S.; Wang, L.; Wang, H. NIR light propulsive Janus-like nanohybrids for enhanced photothermal tumor therapy. *Small* **2016**, *12*, 5423−5430.
(119) Xu, J.; Xu, L.; Wang, C.; Yang, R.; Zhuang, Q.; Han, X.; Dong, Z.; Zhu, W.; Peng, R.; Liu, Z. Near-infrared-triggered photodynamic therapy with multitasking upconversion nanoparticles in combination

with checkpoint blockade for immunotherapy of colorectal cancer. *ACS Nano* **2017**, *11*, 4463−4474.
(120) Zhu, J.; Xiao, T.; Zhang, J.; Che, H.; Shi, Y.; Shi, X.; van Hest, J. C. M. Surface-charge-switchable nanoclusters for magnetic resonance imaging-guided and glutathione depletion-enhanced photodynamic therapy. *ACS Nano* **2020**, *14*, 11225−11237.
(121) Yang, Y. N.; Zhang, M.; Song, H.; Yu, C. Silica-based nanoparticles for biomedical applications: from nanocarriers to biomodulators. *Acc. Chem. Res.* **2020**, *53*, 1545−1556.

https://doi.org/10.1021/acs.chemmater.1c00192
Chem. Mater. 2021, 33, 3022−3046